Electronic supplementary information (ESI) for the manuscript: Complex formation between UO_2^{2+} and α-isosaccharinic acid: insights on a molecular level.

Authors: Hannes Brinkmann, Michael Patzschke, Peter Kaden, Manuel Raiwa, André Rossberg, Roger Kloditz, Karsten Heim, Henry Moll, Thorsten Stumpf

1 Synthesis of NaISA

1.1 ESI-MS

ESI-MS was used to check the purity of the synthesized NaISA stock solution. Fig. SI 1 shows the ESI-MS spectrum of a 15 mM NaISA solution at pH 4. Tab. SI 1 summarizes the dominant compounds considering all signals with a relative intensity larger than 2 %. All signals can be assigned to HISA- and/or ISA-containing compounds and no impurities were detected. Furthermore, this shows the stability of the ligand during the ionization process and in the gas phase.

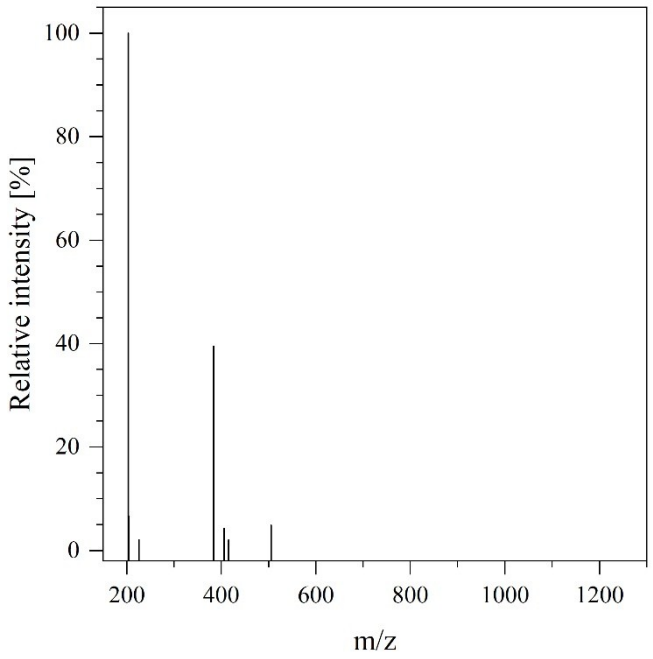

Fig. SI 1: ESI-MS spectrum of a 15 mM NaISA solution at pH 4.

Tab. SI 1: ESI-MS data of the NaISA stock solution (15 mM, pH 4).

m/z (Intensity [%])	Assignment
203 (100)	$[^{23}Na(^{12}C_6H_{12}O_6)]^+$
383 (39)	$[^{23}Na(^{12}C_6H_{12}O_6)_2]^+$
204 (7)	$[^{23}Na(^{13}C^{12}C_5H_{12}O_6)]^+$
384 (5)	$[^{23}Na(^{13}C^{12}C_5H_{12}O_6)\ (^{12}C_6H_{12}O_6)_2]^+$
505 (5)	$[^{23}Na_2{}^{35}ClO_4(^{12}C_6H_{12}O_6)_2]^+$
405 (4)	$[^{23}Na_2(^{12}C_6H_{12}O_6)(^{12}C_6H_{11}O_6)]^+$
225 (2)	$[^{23}Na_2(^{12}C_6H_{11}O_6)]^+$
415 (2)	$[(^{12}C_6H_{12}O_6)_2(H_2O)_2(H_3O)]^+$

1.2 NMR spectroscopy

^1H and ^{13}C spectra as well as two-dimensional multiplicity edited $^1H,^{13}C$-HSQC spectra of 50 mM NaISA solutions at pH 2.2, 4.2 and 10.0 were recorded (Fig. SI 2-Fig. SI 17). HSQC spectra are particularly suitable to assign signals to the corresponding proton and carbon nuclei of ISL, HISA or ISA. The carboxylic carbon (1) and the carbon of the tertiary alcohol (2) show no correlation in the HSQC spectrum, since no proton is directly attached. Due to the two adjacent electron withdrawing oxygen atoms, carbon 1 shows the largest chemical shift. Carbon 3 has no adjacent electron withdrawing oxygen atom and shows therefore the smallest chemical shift. The same is valid for the two corresponding protons (3a and 3b). The remaining carbon nuclei have one adjacent oxygen atom and occur in a small range. However, they can be distinguished based on their corresponding ^1H-signal, and hence the resulting signal in the HSQC spectrum. Carbon 4 has one attached proton (4) and shows therefore the sole opposite phased (red) signal in the multiplicity edited $^1H,^{13}C$-HSQC spectrum. The protons 5a and 5b give a pair of doublets of doublets, whereas 6a and 6b give a pair of doublets, which allows the differentiation between carbon 5 and 6.

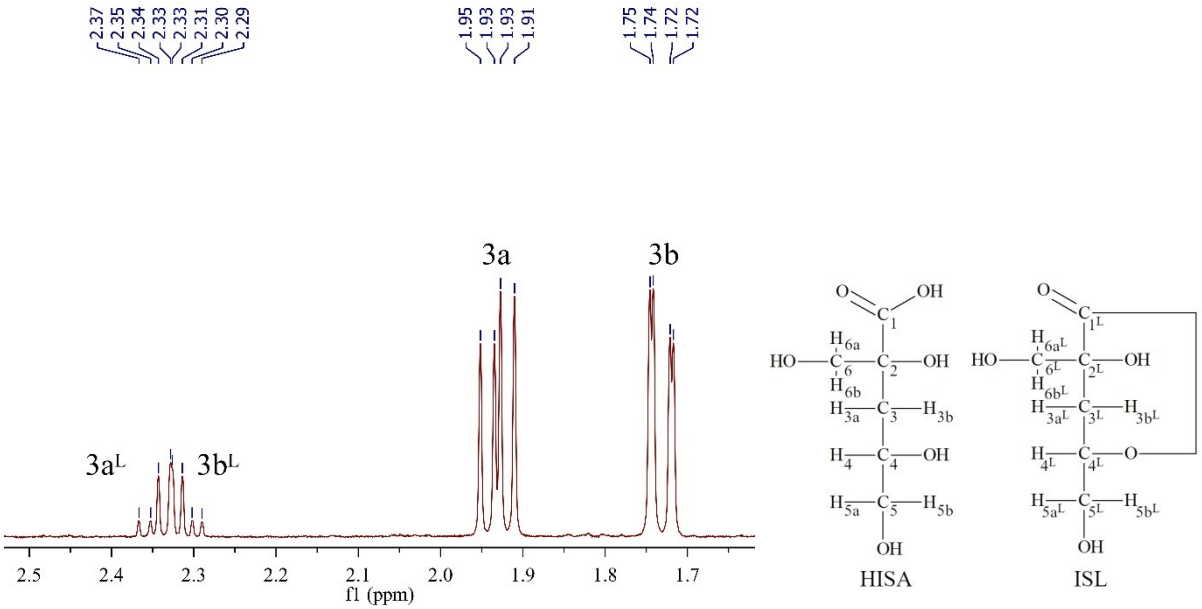

Fig. SI 2: Part one of the ^{1}H spectrum of a 50 mM NaISA solution at **pH 2.2**.

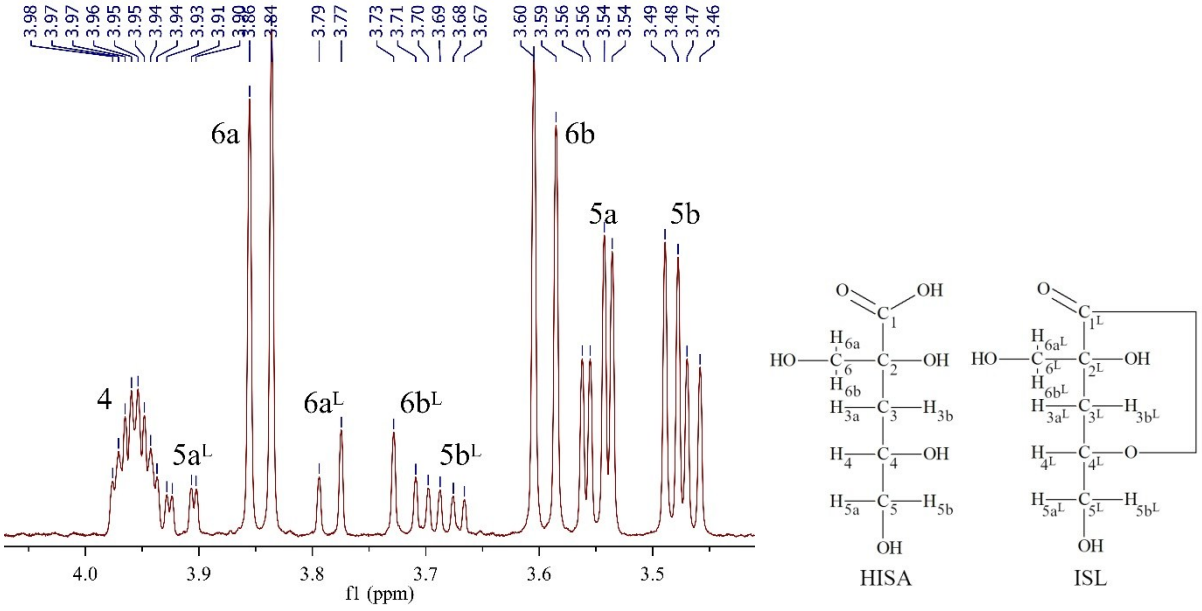

Fig. SI 3: Part two of the ^{1}H spectrum of a 50 mM NaISA solution at **pH 2.2**.

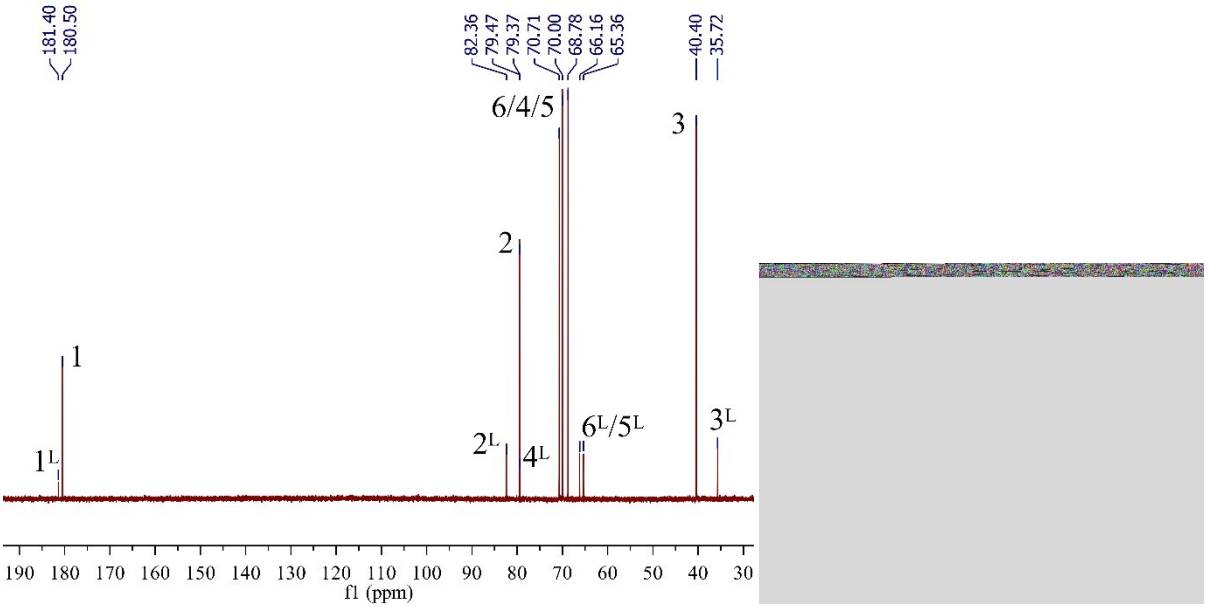

Fig. SI 4: ^{13}C spectrum of a 50 mM NaISA solution at **pH 2.2**.

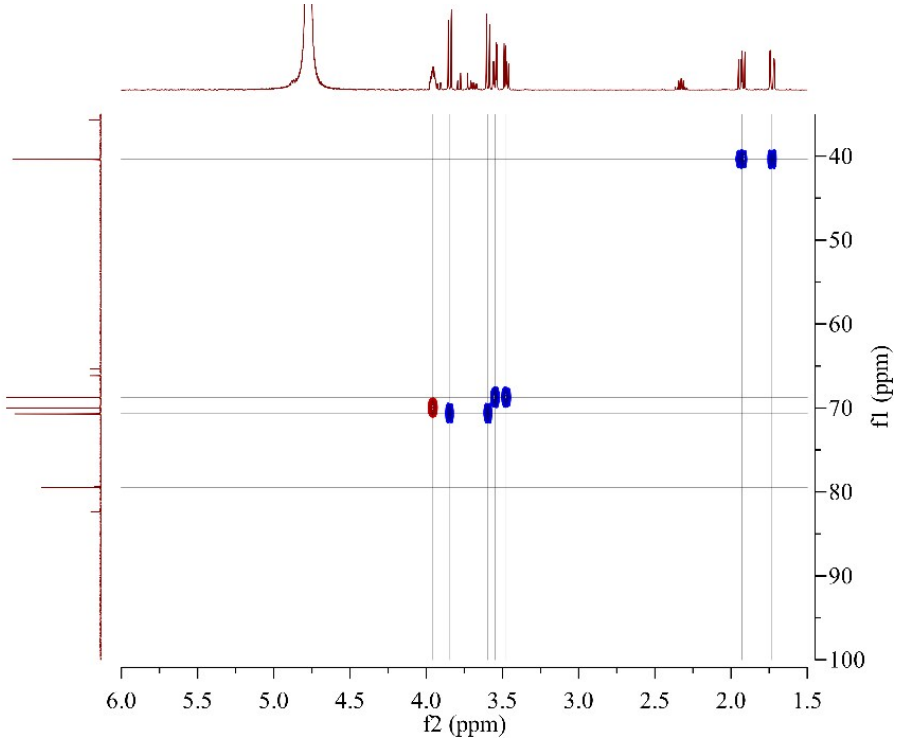

Fig. SI 5: $^{1}H,^{13}C$-HSQC spectrum of a 50 mM NaISA solution at **pH 2.2**.

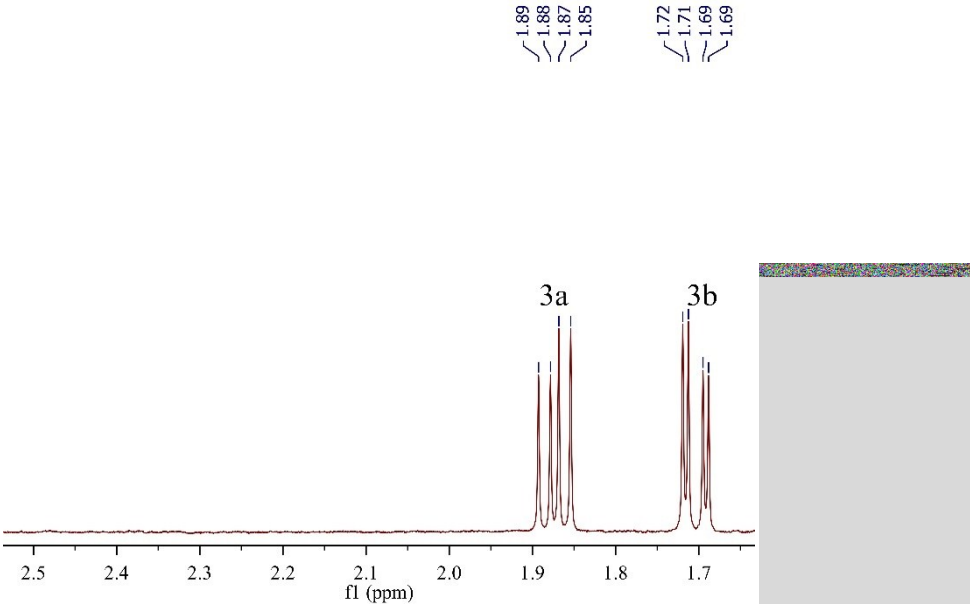

Fig. SI 6: Part one of the ^{1}H spectrum of a 50 mM NaISA solution at **pH 4.2**.

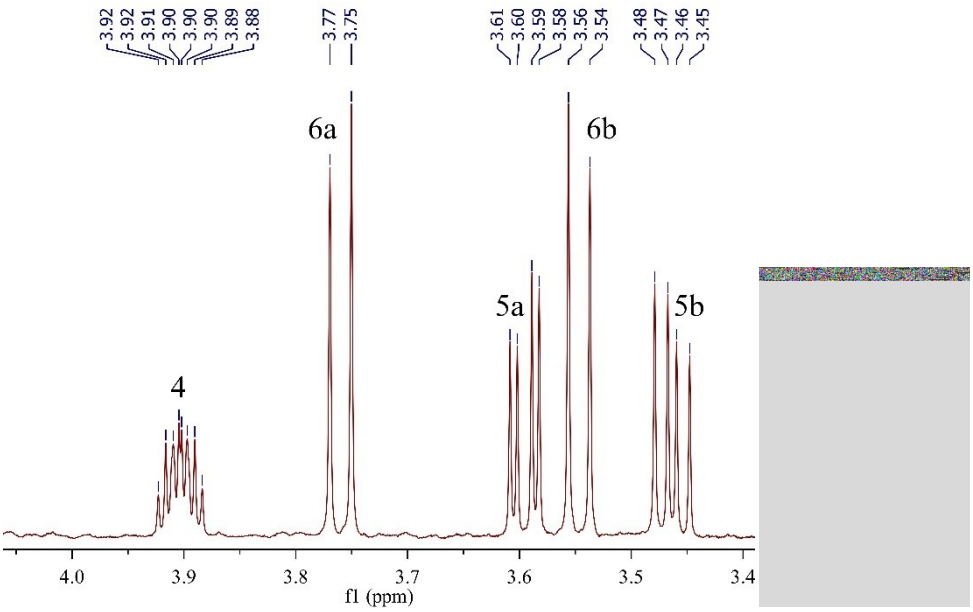

Fig. SI 7: Part two of the ^{1}H spectrum of a 50 mM NaISA solution at **pH 4.2**.

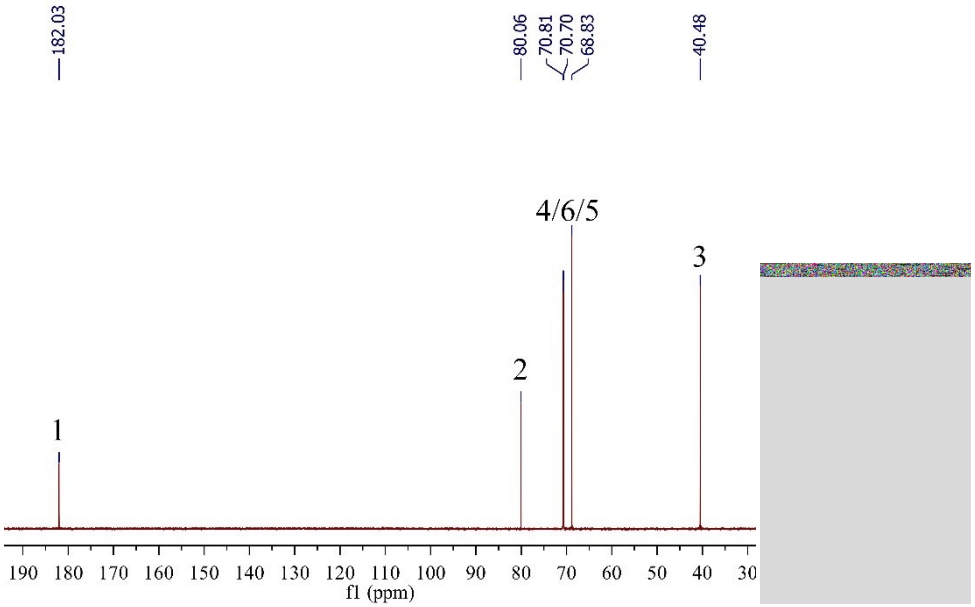

Fig. SI 8: ^{13}C spectrum of a 50 mM NaISA solution at **pH 4.2**.

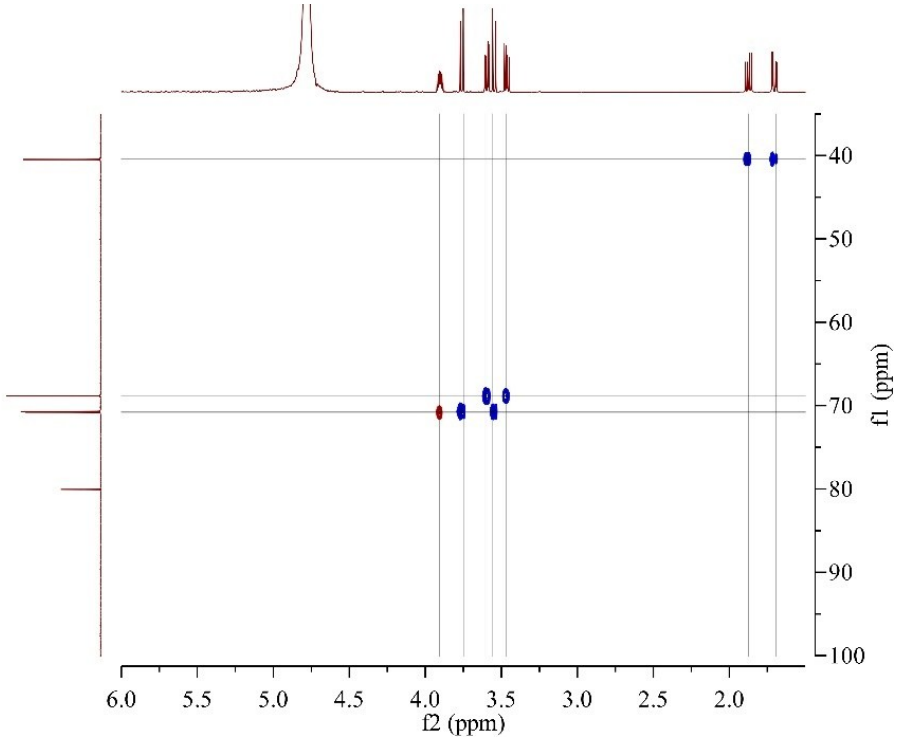

Fig. SI 9: $^{1}H,^{13}C$-HSQC spectrum of a 50 mM NaISA solution at **pH 4.2**.

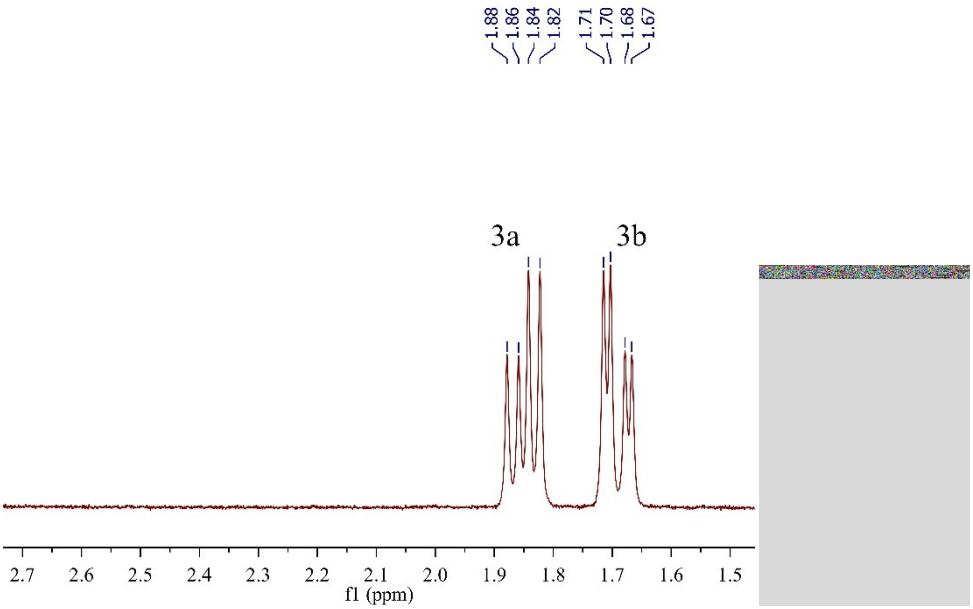

Fig. SI 10: Part one of the ^{1}H spectrum of a 50 mM NaISA solution at **pH 10.0**.

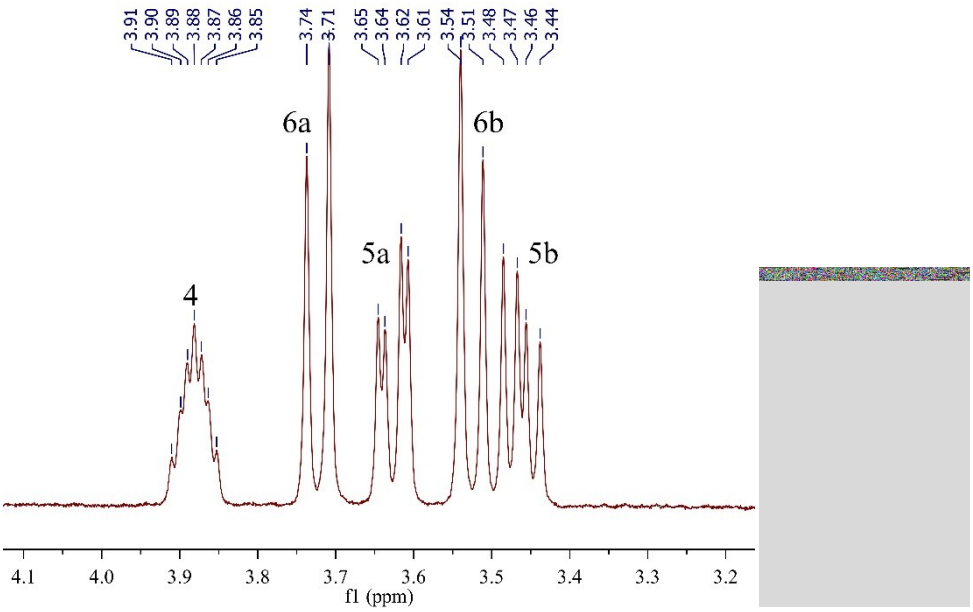

Fig. SI 11: Part two of the ^{1}H spectrum of a 50 mM NaISA solution at **pH 10.0**.

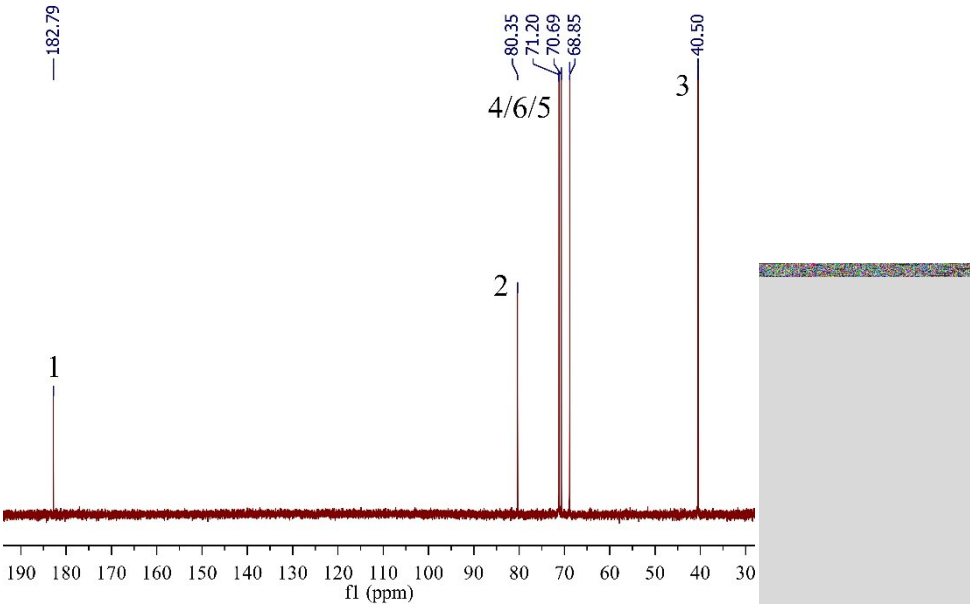

Fig. SI 12: ^{13}C spectrum of a 50 mM NaISA solution at **pH 10.0**.

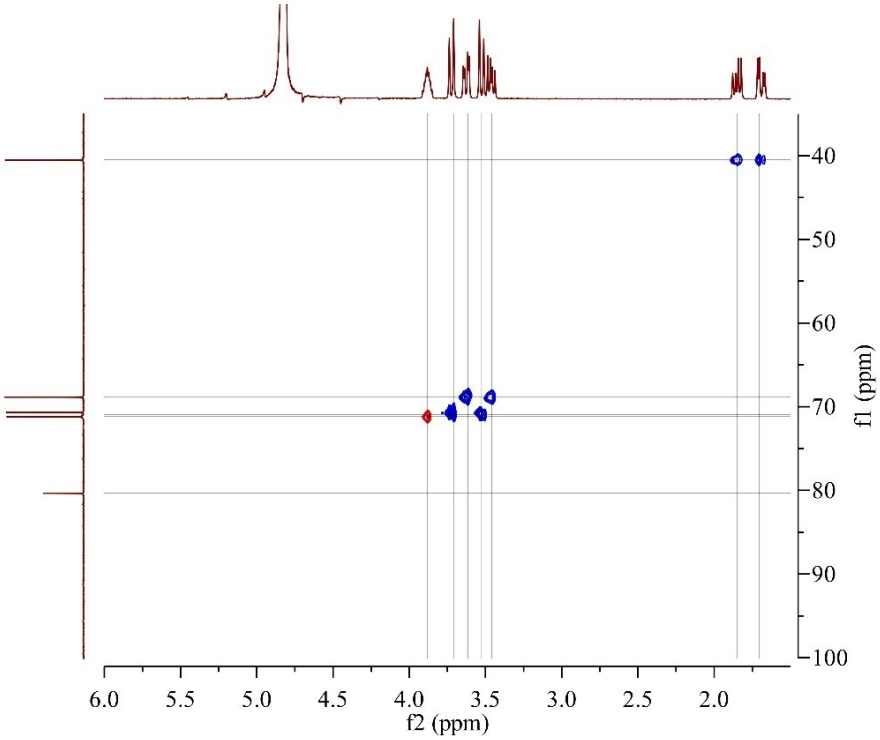

Fig. SI 13: $^{1}H,^{13}C$-HSQC spectrum of a 50 mM NaISA solution at **pH 10.0**.

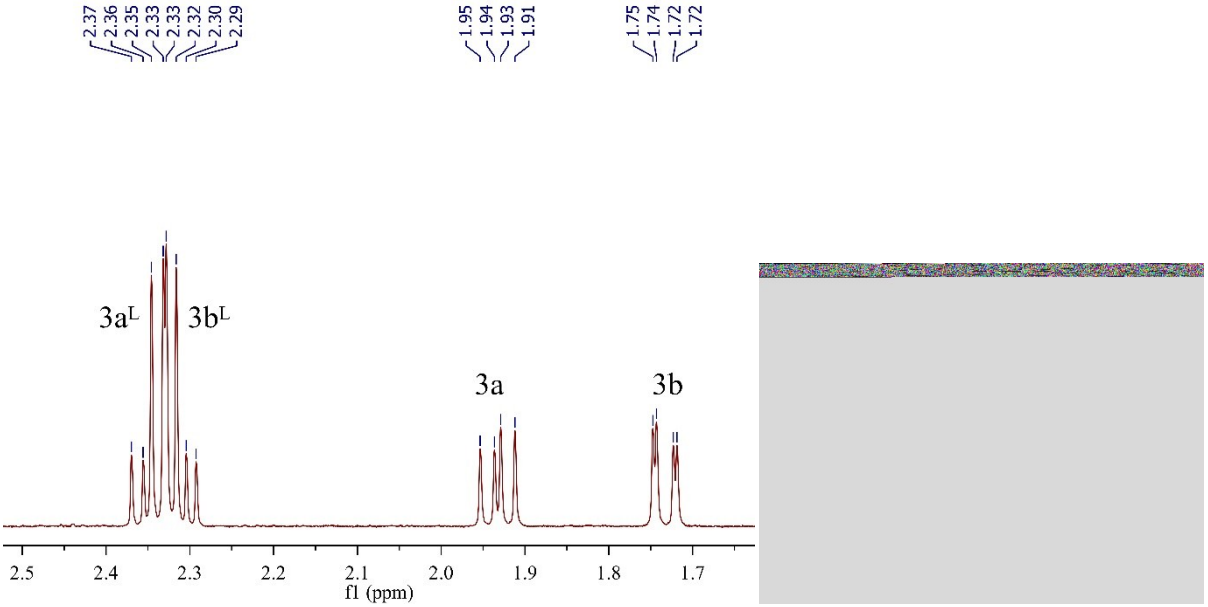

Fig. SI 14: Part one of the ^{1}H spectrum of a 50 mM NaISA solution at **pH 2.2 (8 days after preparation)**.

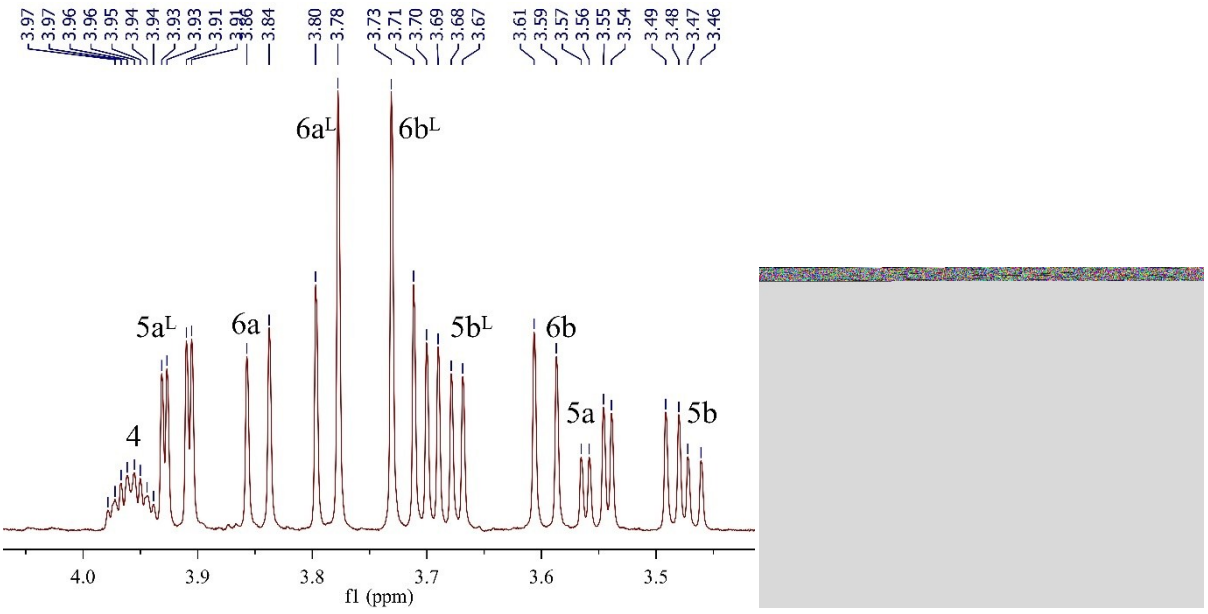

Fig. SI 15: Part two of the ^{1}H spectrum of a 50 mM NaISA solution at **pH 2.2 (8 days after preparation)**.

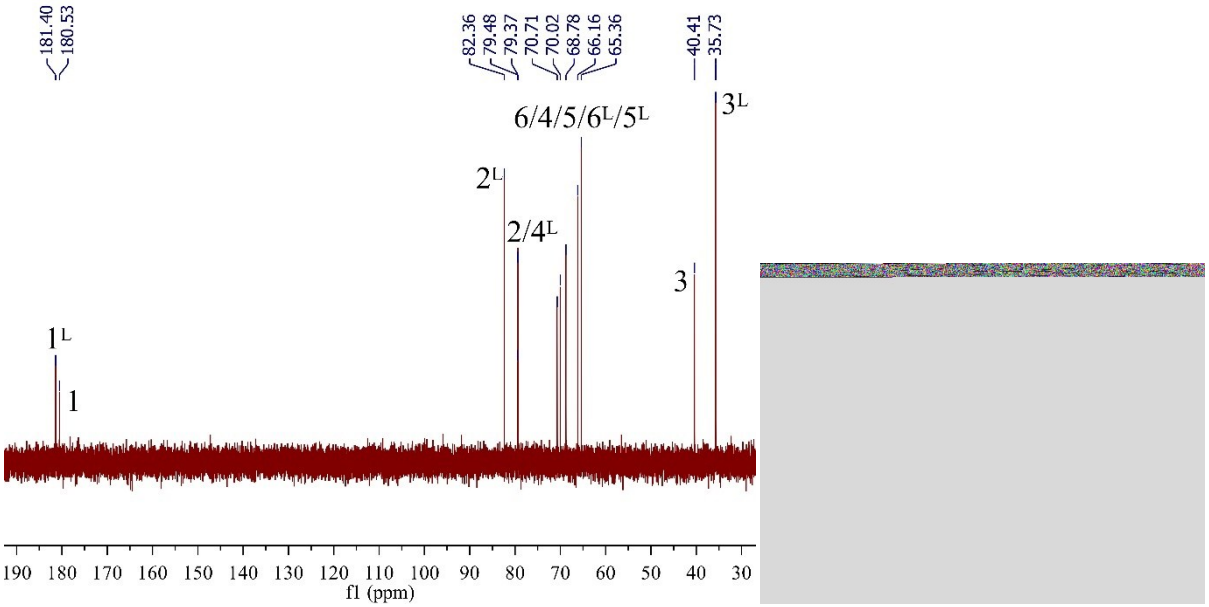

Fig. SI 16: ^{13}C spectrum of a 50 mM NaISA solution at **pH 2.2 (8 days after preparation)**.

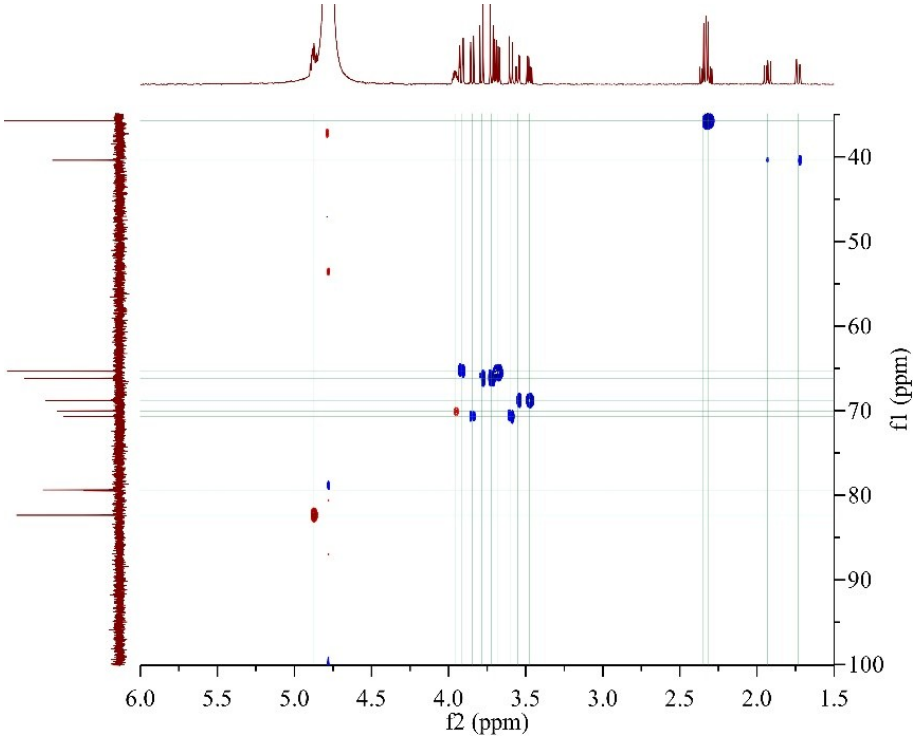

Fig. SI 17: $^{1}H,^{13}C$-HSQC spectrum of a 50 mM NaISA solution at **pH 2.2 (8 days after preparation)**.

Tab. SI 2: ^{13}C signals of 50 mM NaISA solutions at different pH values (present study).

Carbon	δ(^{13}C) of HISA/ISA [ppm]			δ(^{13}C) of ISL [ppm]
	pH 2.2	pH 4.2	pH 10.0	pH 2.2 (8 days after preparation)
1	180.5	182.0	182.8	181.4
2	79.4	80.1	80.4	79.5
3	40.4	40.5	40.5	35.7
4	70.0	70.8	71.2	82.4
5	68.7	68.9	68.9	65.4
6	70.7	70.7	70.9	66.2

Tab. SI 3: ^{1}H signals of 50 mM NaISA solutions at different pH values (present study).

Proton	δ(^{1}H) of HISA/ISA [ppm]			δ(^{1}H) of ISL [ppm]
	pH 2.2	pH 4.2	pH 10.0	pH 2.2 (8 days after preparation)
3a/3b (dd/dd)	1.93/1.73	1.87/1.70	1.85/1.69	2.34/2.32
4 (m)	3.96	3.90	3.88	4.87
5a/5b (dd/dd)	3.55/3.47	3.60/3.46	3.63/3.46	3.92/3.68
6a/6b (d/d)	3.85/3.59	3.76/3.55	3.72/3.53	3.78/3.72

Tab. SI 4: Literature NMR data for ISL.

Carbon	δ(^{13}C) of ISL [ppm]		Proton	δ(^{1}H) of ISL [ppm]	
	Shaw[1]	Cho *et al.*[2]		Shaw[1]	Glaus *et al.*[3]
1	178.6	178.84	-	-	
2	76.6	76.78			
3	32.9	33.14	3a/3b (dd/dd)	2.35/2.29	2.25/2.23
4	79.6	79.79	4 (m)	4.86	4.79
5	63.3; 62.5	63.58; 62.77	5a/5b (dd/dd)	3.91/3.67	3.82/3.59
6			6a/6b (d/d)	3.78/3.71	3.69/3.63

Tab. SI 5: Literature NMR data for HISA/ISA.

Carbon	δ(^{13}C) of HISA/ISA [ppm]	Proton	δ(^{1}H) of HISA/ISA [ppm]	
	Shaw[1]		Shaw[1]	Glaus *et al.*[3]
1	180.0	-	-	
2	77.8			
3	37.6	3a/3b (dd/dd)	1.76/1.60	1.76/1.61
4	68.4; 67.9; 66.0	4 (m)	3.79	3.79
5		5a/5b (dd/dd)	3.52/3.37	3.53/3.37
6		6a/6b (d/d)	3.63/3.44	3.63/3.43

The experimentally determined chemical shifts in Tab. SI 2 and Tab. SI 3 are in very good agreement with literature data from Shaw, Glaus *et al*. and *Cho* et al. (Tab. SI 4 and Tab. SI 5).[1–3] Deviations can be traced back to different reference substances (TMSP in the present study; acetone and $CDCl_3$[1]; water and acetone[3]; TMS[2]) and different pH values. The pH dependency of ^{13}C chemical shifts of ISA was described by Cho *et al*., who showed a downfield shift with increasing pH.[2] No indications for impurities were detected by NMR spectroscopic measurements.

2 Influence of UO_2^{2+} on ISL-formation

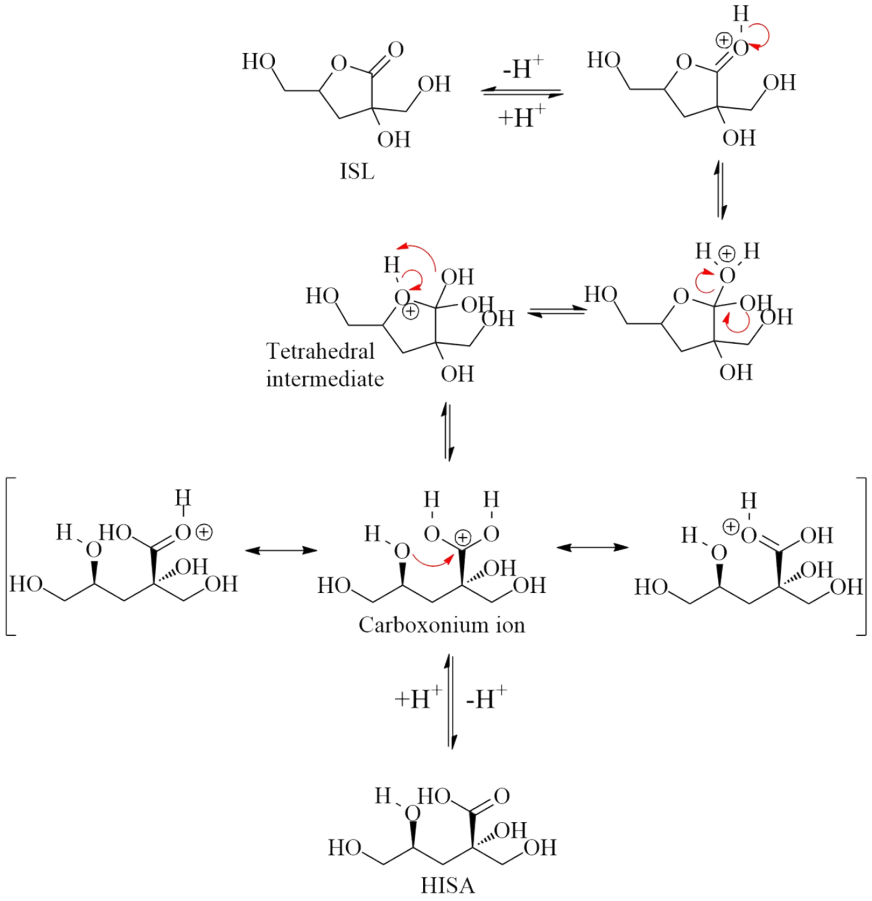

Fig. SI 18: Transformation from HISA to ISL via a proton initiated nucleophilic substitution reaction (general mechanism was adopted from Brückner[4]).

If the carbonyl oxygen of the protonated carboxylic group gets protonated, a resonance stabilized carboxonium ion is formed, which is an excellent acylating agent. The induced positive charge at the carboxylic carbon facilitates the nucleophilic attack of the oxygen atom from the secondary alcohol. Forming this tetrahedral intermediate is the rate limiting step of this reaction. Subsequent rearrangements as well as the cleavage of H_2O finally lead to the formation of ISL.

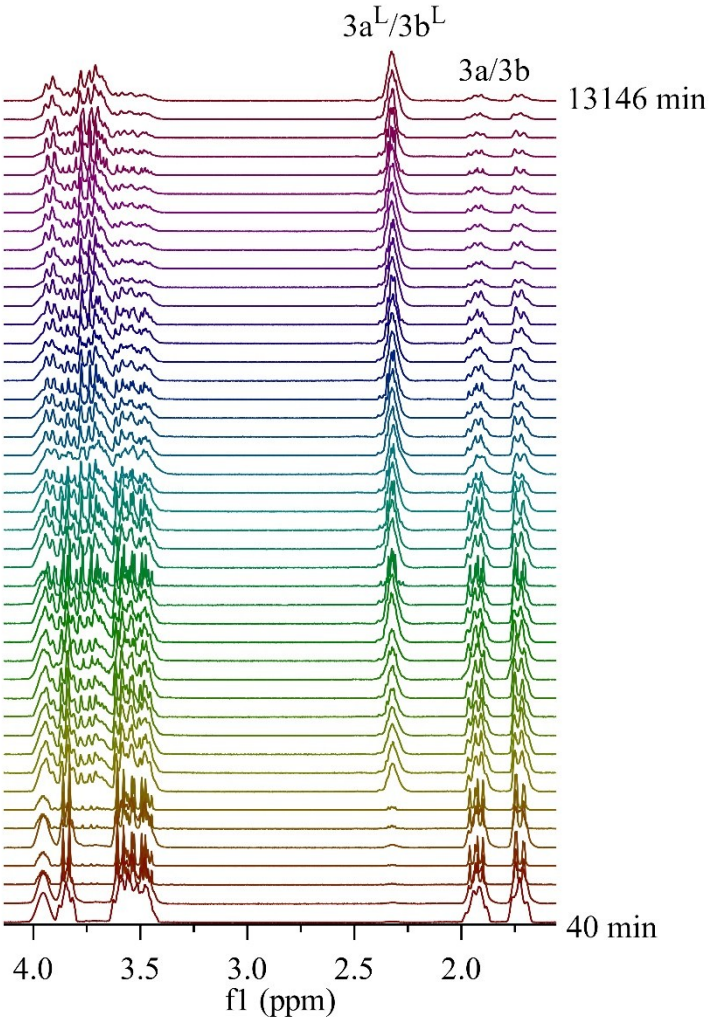

Fig. SI 19: ^{1}H NMR spectra of a 60 mM NaISA solution in the absence of UO_2^{2+} at different time points (see Tab. SI 6).

Tab. SI 6: Lactone formation in the absence of UO_2^{2+}: integrated intensities of the signals 3a/3b and $3a^L/3b^L$ and calculated relative concentrations of HISA and ISL.

Time after preparation [min]	I_{ISL} [a.u.]	I_{HISA} [a.u.]	$I_{ISL}+I_{HISA}$ [a.u.]	$[ISL]_{rel}$	$[HISA]_{rel}$
40	0.02	6.22	6.24	0.00321	0.99679
57	0.02	6.35	6.37	0.00314	0.99686
84	0.04	6.22	6.26	0.00639	0.99361
112	0.06	6.18	6.24	0.00962	0.99038
138	0.10	6.33	6.43	0.01555	0.98445
233	0.21	5.97	6.18	0.03398	0.96602
260	0.25	6.09	6.34	0.03943	0.96057
1204	1.41	4.85	6.26	0.22524	0.77476
1256	1.46	4.87	6.33	0.23065	0.76935
1282	1.53	4.94	6.47	0.23648	0.76352

1306	1.53	4.79	6.32	0.24209	0.75791
1344	1.53	4.68	6.21	0.24638	0.75362
1369	1.61	4.81	6.42	0.25078	0.74922
1398	1.58	4.65	6.23	0.25361	0.74639
1422	1.59	4.65	6.24	0.25481	0.74519
2634	2.22	3.87	6.09	0.36453	0.63547
2658	2.28	3.88	6.16	0.37013	0.62987
2683	2.30	3.85	6.15	0.37398	0.62602
2805	2.34	3.79	6.13	0.38173	0.61827
2849	2.45	3.89	6.34	0.38644	0.61356
2944	2.4	3.63	6.03	0.39801	0.60199
3004	2.49	3.69	6.18	0.40291	0.59709
3175	2.59	3.66	6.25	0.4144	0.5856
4060	3.09	3.06	6.15	0.50244	0.49756
4106	3.14	3.04	6.18	0.50809	0.49191
4309	3.15	2.94	6.09	0.51724	0.48276
4540	3.25	2.84	6.09	0.53366	0.46634
5496	3.52	2.59	6.11	0.5761	0.4239
5526	3.51	2.57	6.08	0.5773	0.4227
5627	3.59	2.51	6.1	0.58852	0.41148
5667	3.65	2.55	6.2	0.58871	0.41129
5724	3.67	2.51	6.18	0.59385	0.40615
5818	3.71	2.53	6.24	0.59455	0.40545
6105	3.75	2.42	6.17	0.60778	0.39222
9808	4.59	1.46	6.05	0.75868	0.24132
9857	4.67	1.5	6.17	0.75689	0.24311
9952	4.60	1.47	6.07	0.75783	0.24217
10013	4.61	1.47	6.08	0.75822	0.24178
10049	4.65	1.44	6.09	0.76355	0.23645
10131	4.63	1.43	6.06	0.76403	0.23597
11458	4.68	1.31	5.99	0.7813	0.2187
12748	5.18	1.35	6.53	0.79326	0.20674
12929	4.84	1.24	6.08	0.79605	0.20395
13036	4.87	1.23	6.1	0.79836	0.20164
13146	5.08	1.24	6.32	0.8038	0.1962

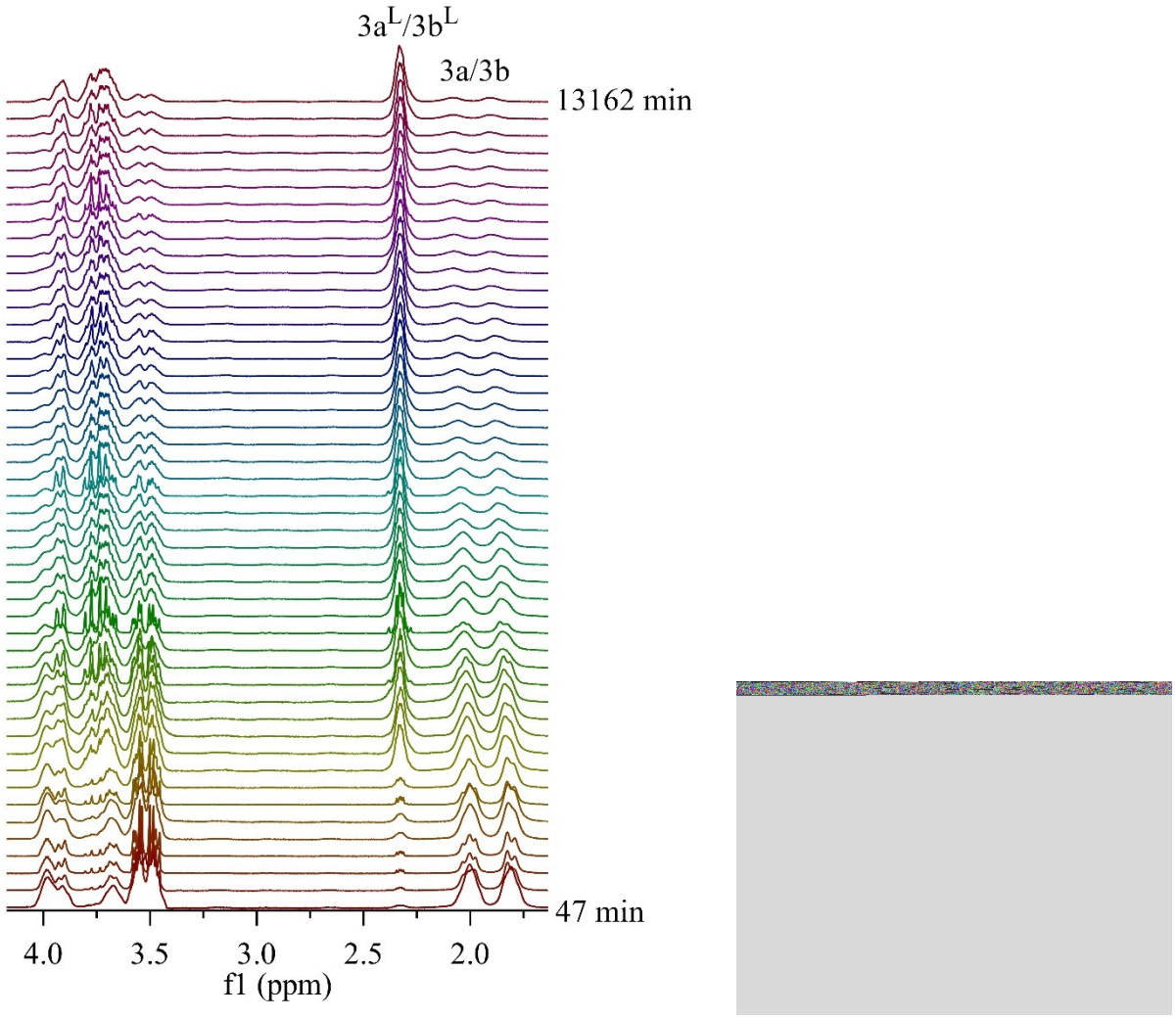

Fig. SI 20: ^{1}H NMR spectra of a 60 mM NaISA solution in the presence of 15 mM UO_2^{2+} at different time points (see Tab. SI 7).

Tab. SI 7: Lactone formation in the presence of UO_2^{2+}: integrated intensities of the signals 3a/3b and $3a^L/3b^L$ and calculated relative concentrations of HISA and ISL.

Time after preparation [min]	I_{ISL} [a.u.]	I_{HISA} [a.u.]	$I_{ISL}+I_{HISA}$ [a.u.]	$[ISL]_{rel}$	$[HISA]_{rel}$
47	0.09	5.77	5.86	0.01536	0.98464
75	0.16	5.77	5.93	0.02698	0.97302
102	0.2	5.73	5.93	0.03373	0.96627
130	0.27	5.75	6.02	0.04485	0.95515
155	0.31	5.64	5.95	0.0521	0.9479
195	0.36	5.58	5.94	0.06061	0.93939
224	0.42	5.53	5.95	0.07059	0.92941
251	0.5	5.53	6.03	0.08292	0.91708

1221	1.70	4.29	5.99	0.28381	0.71619
1271	1.78	4.28	6.06	0.29373	0.70627
1295	1.8	4.21	6.01	0.2995	0.7005
1359	1.89	4.1	5.99	0.31553	0.68447
1412	2.04	4.29	6.33	0.32227	0.67773
1434	1.99	4.03	6.02	0.33056	0.66944
2648	2.81	3.12	5.93	0.47386	0.52614
2673	2.91	3.24	6.15	0.47317	0.52683
2793	3.13	3.29	6.42	0.48754	0.51246
2838	3.25	3.32	6.57	0.49467	0.50533
2862	3.25	3.35	6.6	0.49242	0.50758
2934	3.22	3.13	6.35	0.50709	0.49291
2993	3.43	3.24	6.67	0.51424	0.48576
3104	3.42	3.06	6.48	0.52778	0.47222
4050	3.91	2.57	6.48	0.6034	0.3966
4074	3.83	2.45	6.28	0.60987	0.39013
4124	3.82	2.37	6.19	0.61712	0.38288
4255	3.95	2.43	6.38	0.61912	0.38088
4567	4.42	2.48	6.9	0.64058	0.35942
5511	4.66	1.94	6.6	0.70606	0.29394
5544	4.54	1.83	6.37	0.71272	0.28728
5615	4.47	1.76	6.23	0.7175	0.2825
5657	4.49	1.76	6.25	0.7184	0.2816
5712	4.61	1.78	6.39	0.72144	0.27856
5750	4.51	1.76	6.27	0.7193	0.2807
5806	4.57	1.83	6.4	0.71406	0.28594
6094	4.76	1.75	6.51	0.73118	0.26882
9823	4.73	1.24	5.97	0.79229	0.20771
9873	4.77	1.26	6.03	0.79104	0.20896
9969	4.89	1.40	6.29	0.77742	0.22258
10028	4.77	1.32	6.09	0.78325	0.21675
10065	4.82	1.17	5.99	0.80467	0.19533
10116	4.77	1.24	6.01	0.79368	0.20632
11476	4.82	1.18	6	0.80333	0.19667
12689	5.01	1.15	6.16	0.81331	0.18669
12736	5.13	1.22	6.35	0.80787	0.19213

12766	5.00	1.12	6.12	0.81699	0.18301
12947	4.86	1.18	6.04	0.80464	0.19536
13134	4.81	1.13	5.94	0.80976	0.19024
13162	4.85	1.11	5.96	0.81376	0.18624

The calculated relative concentrations over time were fitted with the ExpDec1 function of OriginPro 2017G: $y = y_0 + A \cdot e^{-\frac{x}{t_1}}$. The results of the fits are summarized in Tab. SI 8.

Tab. SI 8: Results of the fit of the relative concentrations with the ExpDec1 function.

Series	R^2 [%]	A_0 [%]	A_∞ [%]	k [min^{-1}]	$t_{1/2}$ [min]
HISA without UO_2^{2+}	99.74	98.80	14.37	$2.10 \cdot 10^{-4}$	3294
ISL without UO_2^{2+}	99.76	-0.76	82.69	$2.36 \cdot 10^{-4}$	2934
HISA with UO_2^{2+}	99.76	99.36	17.75	$3.37 \cdot 10^{-4}$	2058
ISL with UO_2^{2+}	99.94	0.71	82.28	$3.36 \cdot 10^{-4}$	2066

R^2	coefficient of determination
$A_0 = y_0 + A$	initial concentration
$A_\infty = y_0$	equilibrium concentration
$k = t_1^{-1}$	rate constant
$t_{1/2} = \ln(2) * t_1$	half life

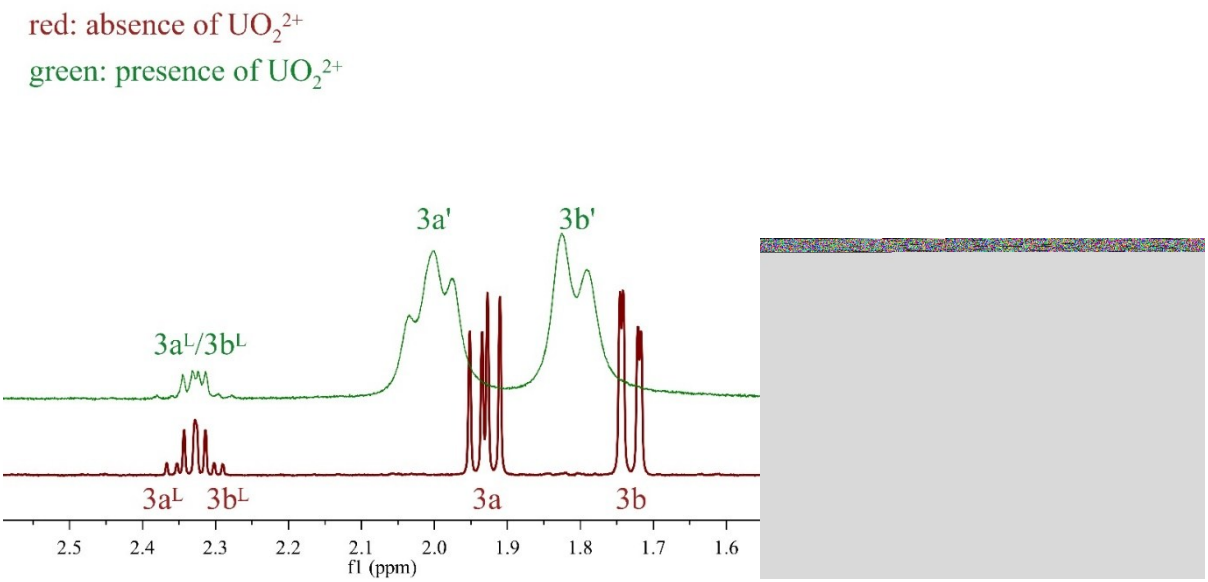

Fig. SI 21: Comparison of ^{1}H-NMR spectra of a UO_2^{2+}-free NaISA sample (50 mM NaISA; pH 2.2; red spectrum) as reference with a UO_2^{2+}-containing sample (15 mM UO_2^{2+}; 60 mM NaISA; pH 2.2; measured 102 min after preparation; green spectrum) (Part one).

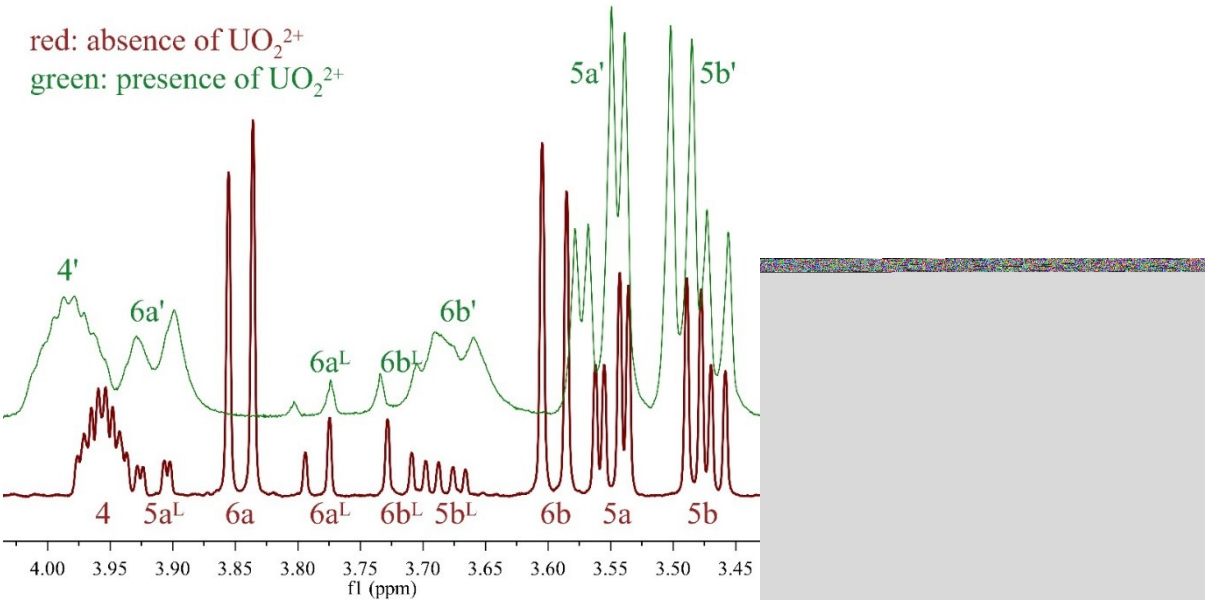

Fig. SI 22: Comparison of ^{1}H-NMR spectra of a UO_2^{2+}-free NaISA sample (50 mM NaISA; pH 2.2; red spectrum) as reference with a UO_2^{2+}-containing sample (15 mM UO_2^{2+}; 60 mM NaISA; pH 2.2; measured 102 min after preparation; green spectrum) (Part two).

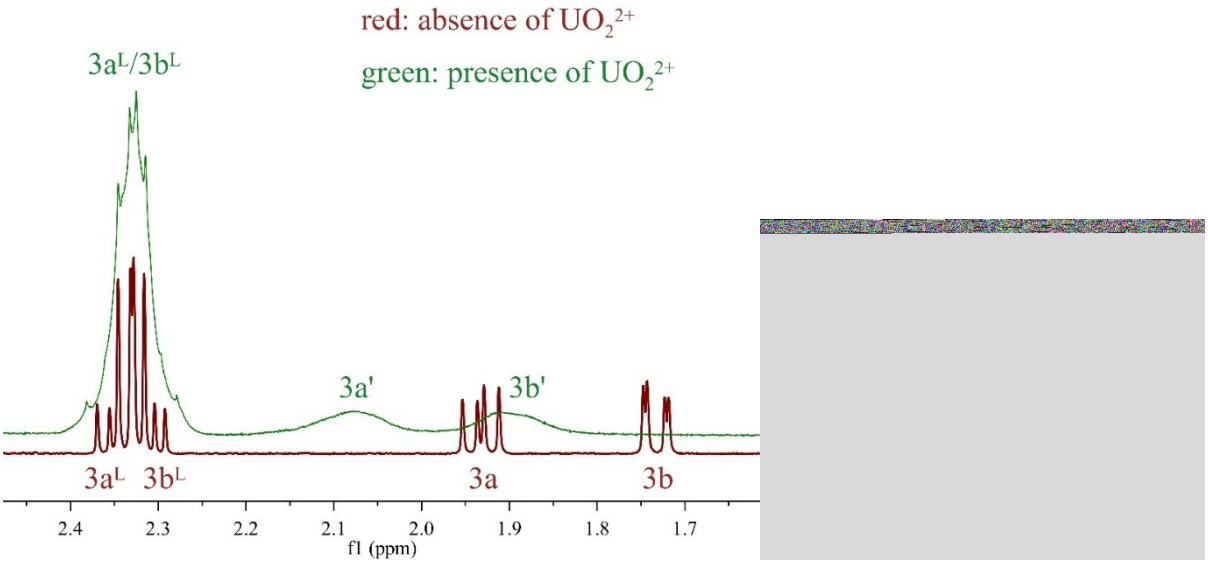

Fig. SI 23: Comparison of ^{1}H-NMR spectra of a UO_2^{2+}-free NaISA sample (50 mM NaISA; pH 2.2; measured 8 days after preparation; red spectrum) as reference with a UO_2^{2+}-containing sample (15 mM UO_2^{2+}; 60 mM NaISA; pH 2.2; measured 10116 min after preparation; green spectrum) (Part one).

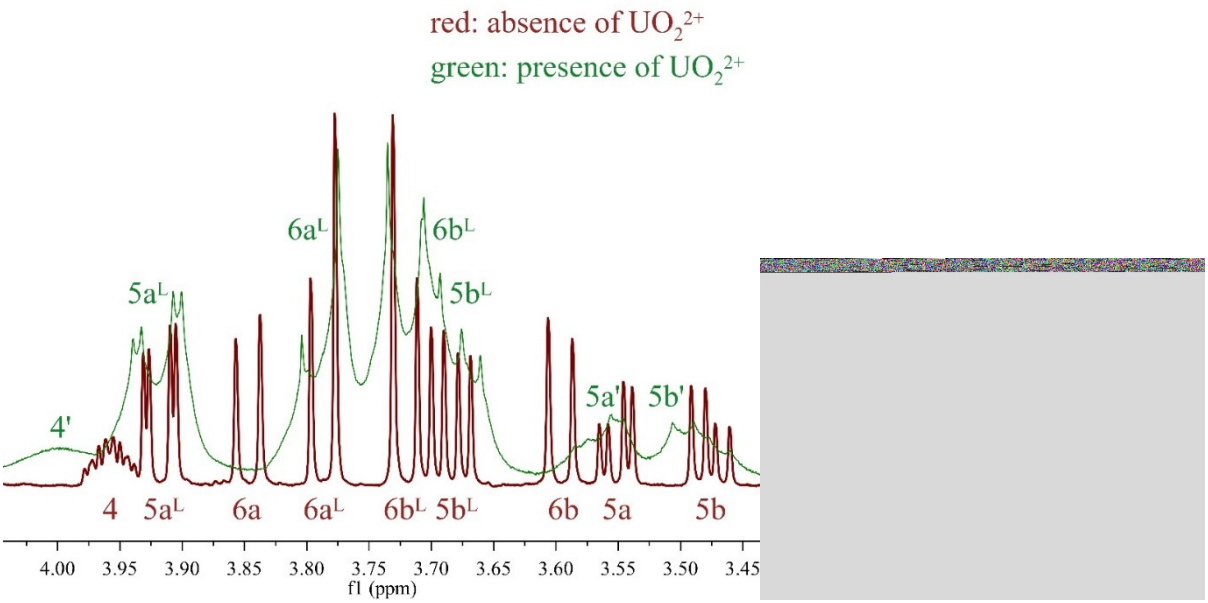

Fig. SI 24: Comparison of ^{1}H-NMR spectra of a UO_2^{2+}-free NaISA sample (50 mM NaISA; pH 2.2; measured 8 days after preparation; red spectrum) as reference with a UO_2^{2+}-containing sample (15 mM UO_2^{2+}; 60 mM NaISA; pH 2.2; measured 10116 min after preparation; green spectrum) (Part two).

3 NMR – Identification of dominant binding sites

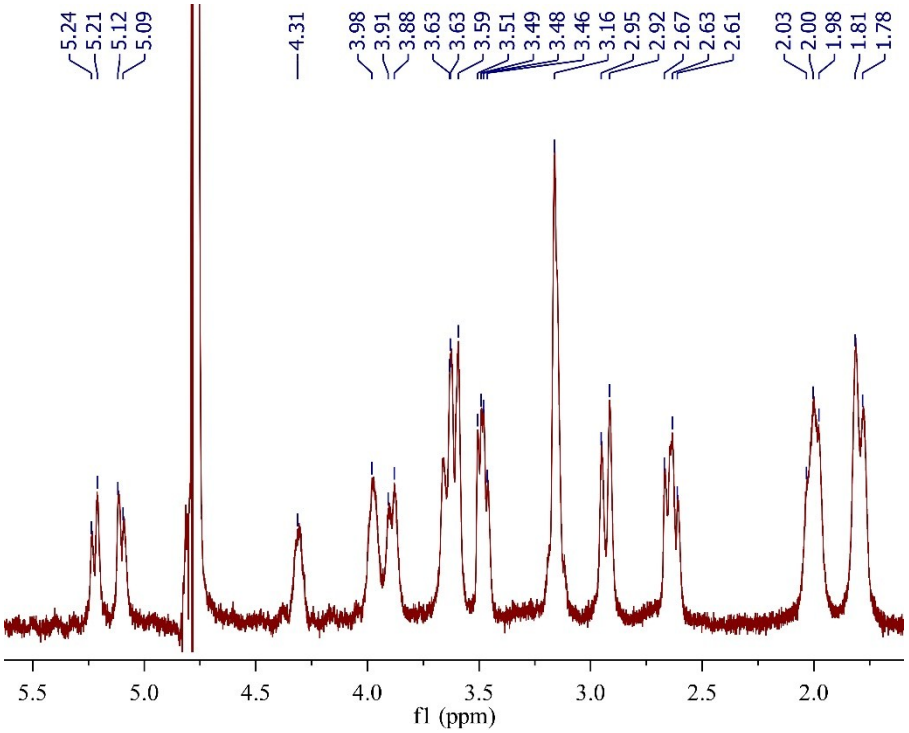

Fig. SI 25: ^{1}H-NMR spectrum of a sample containing 15 mM UO_2^{2+} and 30 mM NaISA at pH 4.2 (spectrum was measured one hour after preparation).

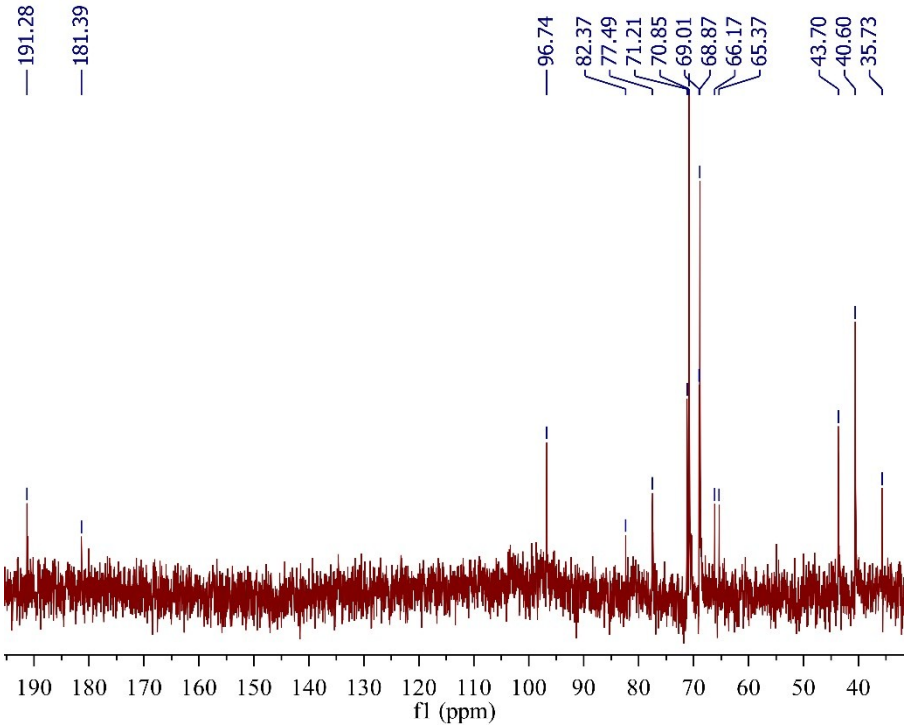

Fig. SI 26: ^{13}C-NMR spectrum of a sample containing 15 mM UO_2^{2+} and 30 mM NaISA at pH 4.2 (several ^{13}C spectra were accumulated over 3 days and averaged).

4 ATR-FTIR spectroscopy

4.1 ATR-FTIR spectra

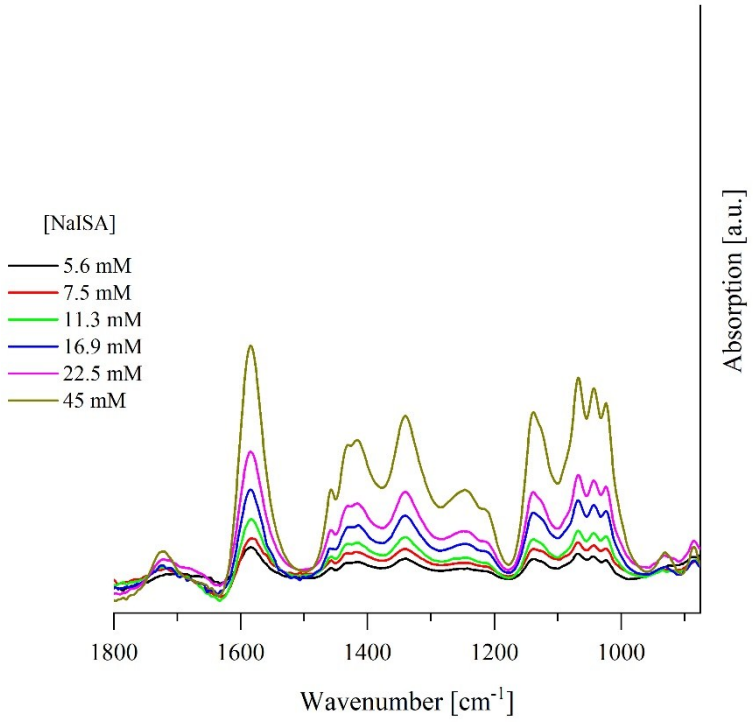

Fig. SI 27: ATR-FTIR spectra of the concentration series (pH 4) in the absence of UO_2^{2+}.

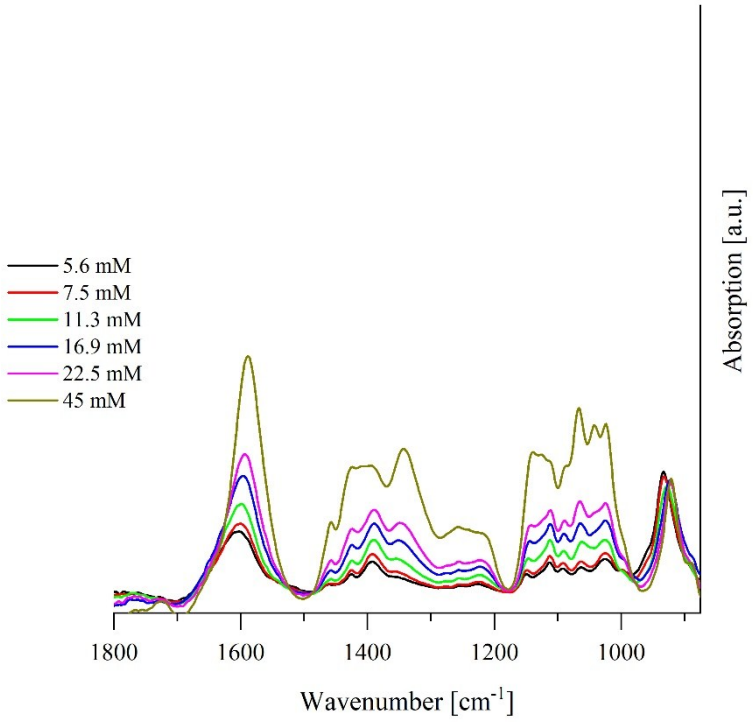

Fig. SI 28: ATR-FTIR spectra of the concentration series (pH 4) in the presence of 11.25 mM UO_2^{2+}.

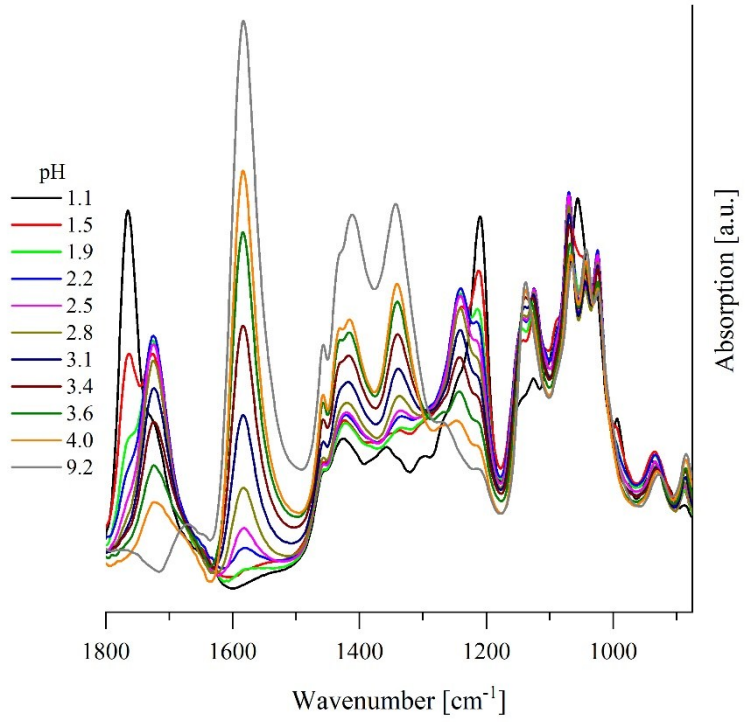

Fig. SI 29: ATR-FTIR spectra of the pH series (90 mM NaISA) in the absence of UO_2^{2+} including the additional sample with pH 9.2.

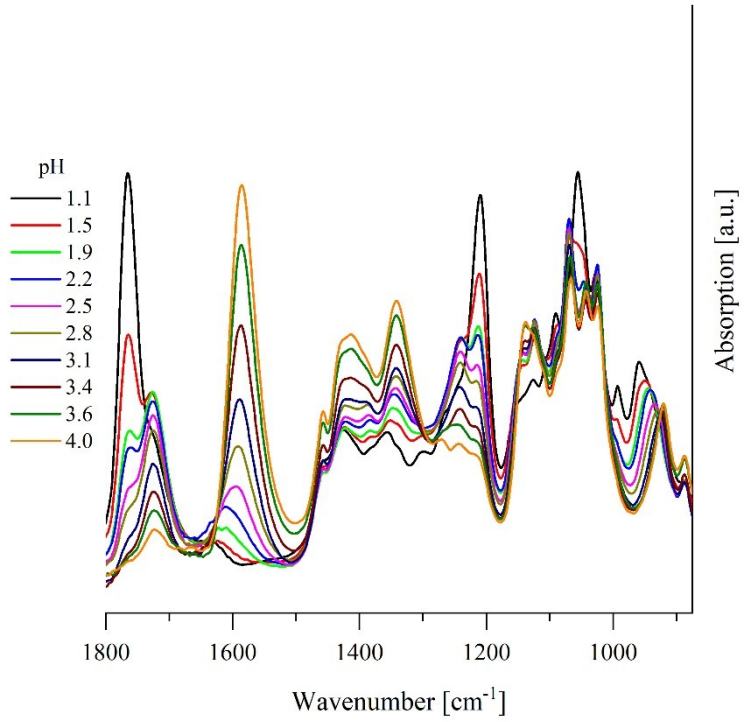

Fig. SI 30: ATR-FTIR spectra of the pH series (90 mM NaISA) in the presence of 11.25 mM UO_2^{2+}.

4.2 Assignment of vibrational modes of ISL, HISA and ISA

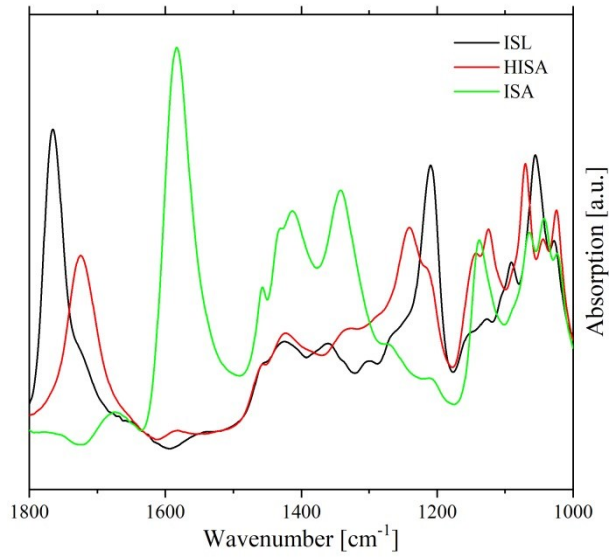

Fig. SI 31: Isolated ATR-FTIR single component spectra of ISL, HISA and ISA.

ISL can unambiguously be identified by the intensive bands at 1765 cm^{-1}, 1209 cm^{-1} and 1055 cm^{-1}, which correspond to the C=O and the C-O-C stretching of the γ-lactone.[5] The carboxylic group of HISA shows the C=O stretching at 1724 cm^{-1} and the mode at 1240 cm^{-1} is associated with the vibration of the C-OH group.[5] Cassanas *et al.*, who focused on lactic acid and lactates, assigned it to the bending and stretching vibrations.[6] The asymmetric (ν_{as}) and symmetric (ν_s) stretching modes of the deprotonated carboxylic group are important to characterize the binding modes in UO_2^{2+}-ISA complexes. ν_{as} is the dominant mode at 1583 cm^{-1}. ν_s occurs in a range where bending modes of the methylene groups with medium to strong intensity are also expected (1480 to 1440 cm^{-1}). Based on reference data for similar components, the mode at 1413 cm^{-1} was assigned to ν_s.[6,7] C-O stretching modes of the different alcohol functionalities cause intensive modes between 1000 cm^{-1} and 1150 cm^{-1}. It is most likely that the modes at 1125 cm^{-1} for HISA and at 1138 cm^{-1} for ISA can be assigned to the tertiary alcohol, since these are expected to occur at higher wavenumbers compared to the secondary and primary alcohols.[5] The expected regions for the latter two functional groups overlap and an unambiguous assignment is therefore not possible.

5 UV-Vis spectroscopy

5.1 Single component spectra from UV-Vis series and spectrum of UO_2^{2+} in the absence of ISA

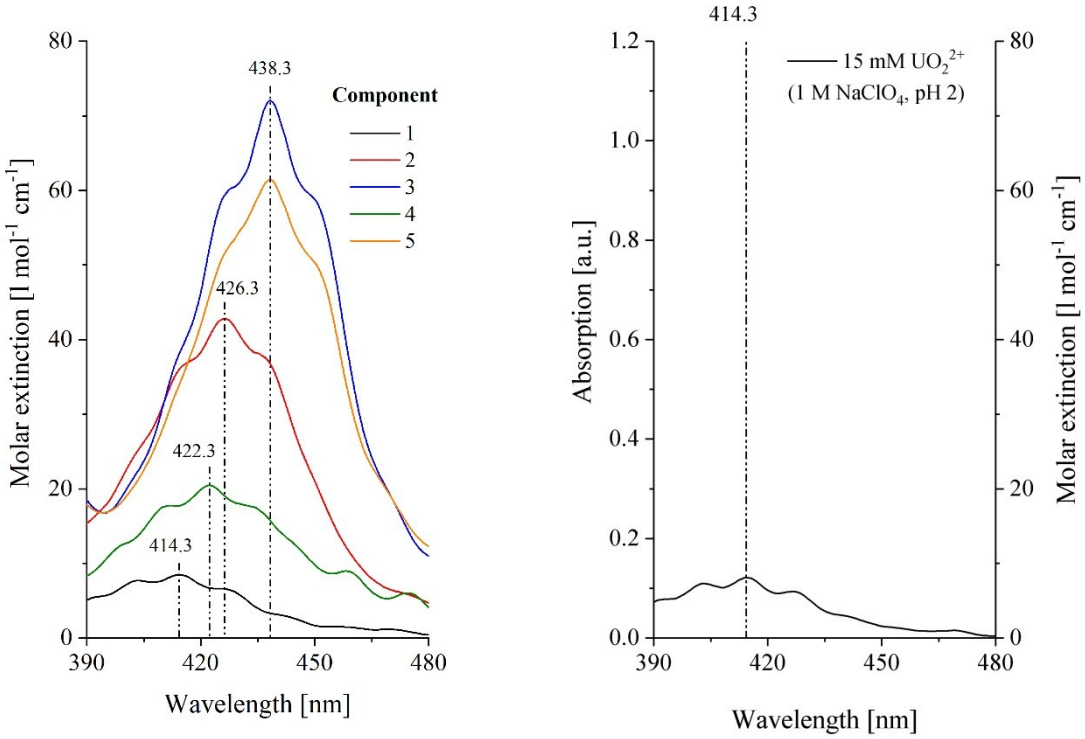

Fig. SI 32: Averaged single component spectra of the five detected components from ITFA evaluation (left) and spectrum of a 15 mM UO_2^{2+} solution at pH 2 in 1 M $NaClO_4$ (right).

5.2 UV-Vis spectra of NMR-samples

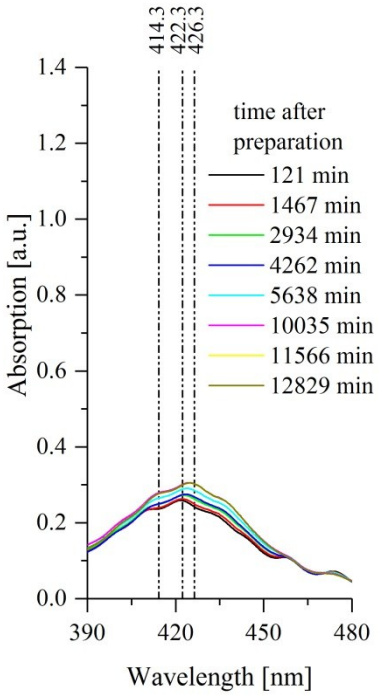

Fig. SI 33: UV-Vis spectra of a UO_2^{2+}-containing NMR-sample (60 mM NaISA; 15 mM UO_2^{2+}; pH 2.2) at different points in time after preparation.

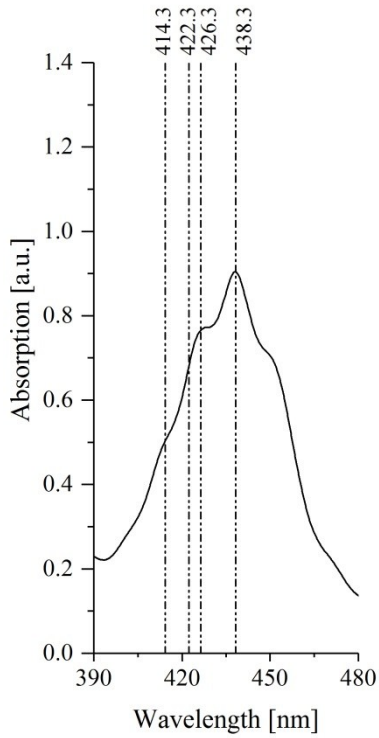

Fig. SI 34: UV-Vis spectrum of a UO_2^{2+}-containing NMR-sample (15 mM UO_2^{2+}; 30 mM NaISA; pH 4.2).

5.3 UV-Vis spectra of ATR-FTIR samples

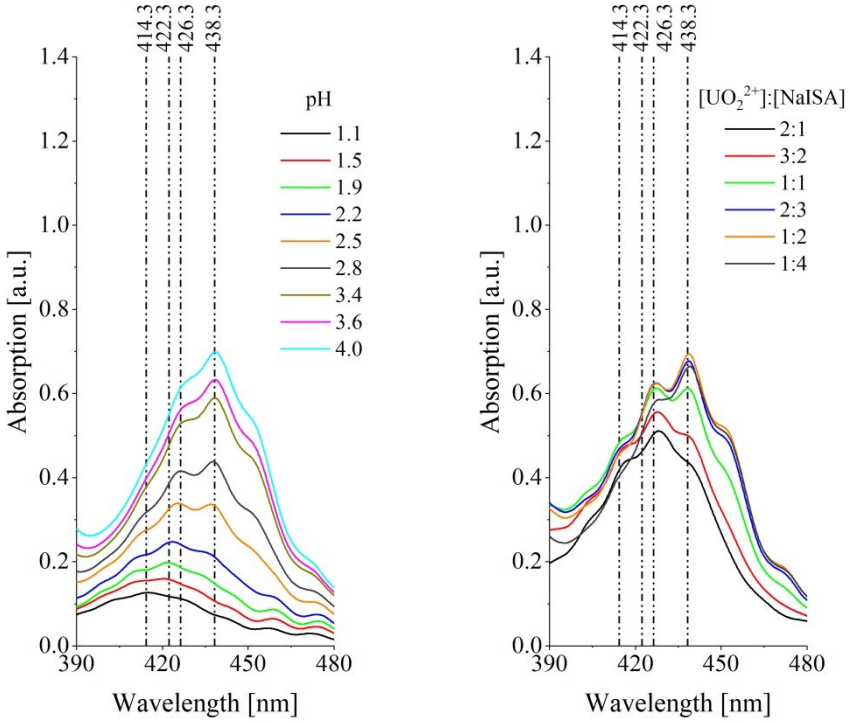

Fig. SI 35: UV-Vis spectra of the UO_2^{2+}-containing ATR-FTIR samples (left: pH series (90 mM NaISA; 11.25 mM UO_2^{2+}); right: concentration series (pH 4; 11.25 mM UO_2^{2+}))

5.4 UV-Vis spectra of ESI-MS samples

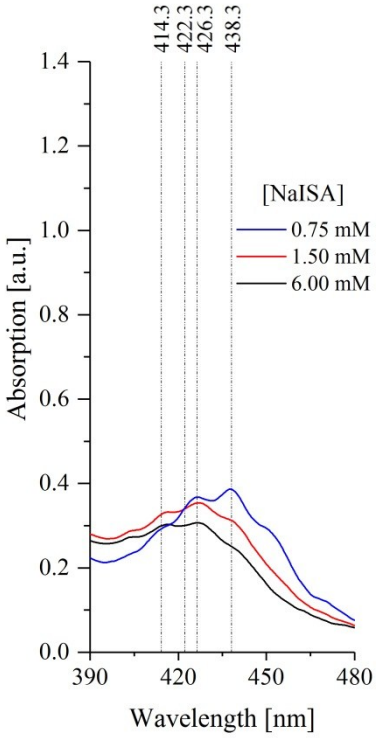

Fig. SI 36: UV-Vis spectra of UO_2^{2+}-containing ESI-MS samples (1.5 mM UO_2^{2+}; pH 4)

5.5 UV-Vis spectra of EXAFS samples

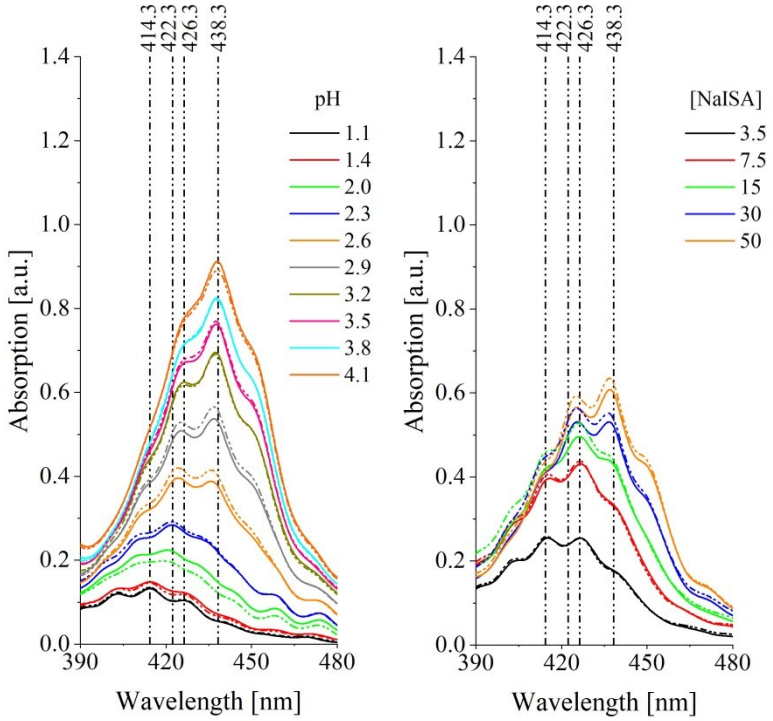

Fig. SI 37: UV-Vis spectra of the EXAFS samples immediately after (solid lines) and 15 days after preparation (dashed lines) (pH series left (15 mM UO_2^{2+}; 90 mM NaISA) and concentration series right (15 mM UO_2^{2+}; pH 3))

6 ESI-MS

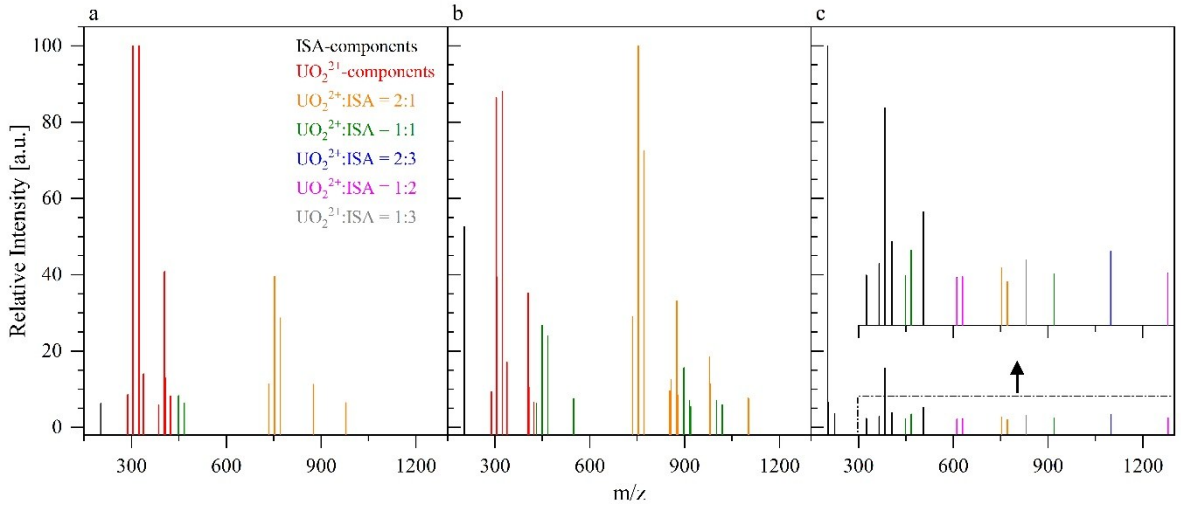

Fig. SI 38: ESI-MS spectra of UO_2^{2+}-ISA samples: 1.5 mM UO_2^{2+} at pH 4 with 0.75 mM (a), 1.5 mM (b) and 6 mM NaISA (c).

7 EXAFS

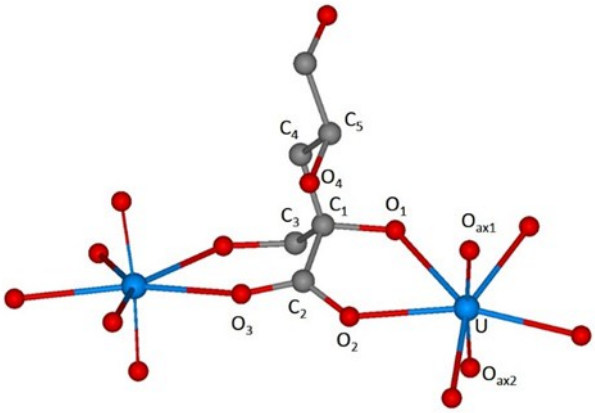

Fig. SI 39: FEFF structural model used for the calculation of theoretical phase and amplitude functions. The assignments of the atoms are explained in the main text.

Tab. SI 9: Chemical composition of the EXAFS samples.

Sample number	pH	$[UO_2^{2+}]$ [mM]	[NaISA] [mM]	Series
1	1.0	15	90	pH series
2	2.0	15	90	
3	2.3	15	90	
4	2.6	15	90	
5	2.9	15	90	
6	3.2	15	90	
7	3.5	15	90	
8	4.1	15	90	
9	3.0	15	3.5	Concentration series
10	3.0	15	7.5	
11	3.0	15	15	
12	3.0	15	30	
13	3.0	15	50	

Tab. SI 10: Indicator function (IND) in dependence on the number of spectral components (n) used for the reconstruction of the EXAFS spectral mixtures. The components 8-13 were omitted.

n	IND(n)·10^4
1	18.6
2	7.7
3	6.5
4	6.8

5	7.6
6	8.4
7	10.5

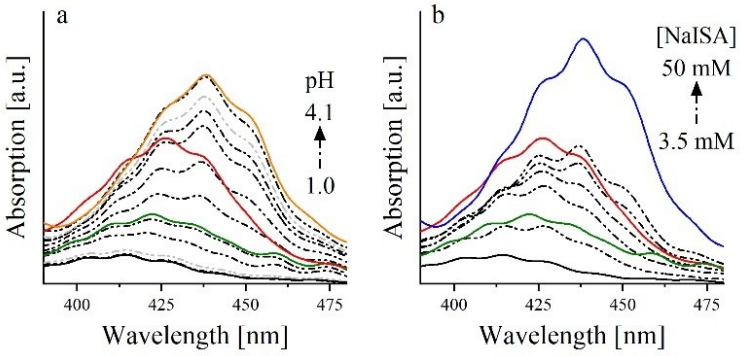

Fig. SI 40: Measured UV-Vis spectra of the EXAFS samples (dashed lines): (a) pH series (no EXAFS measurements were performed for the samples with the grey dashed lines) and (b) concentrations series. The solid lines are the single component spectra of Fig. SI 32, which were used as reference data for the ITFA evaluation.

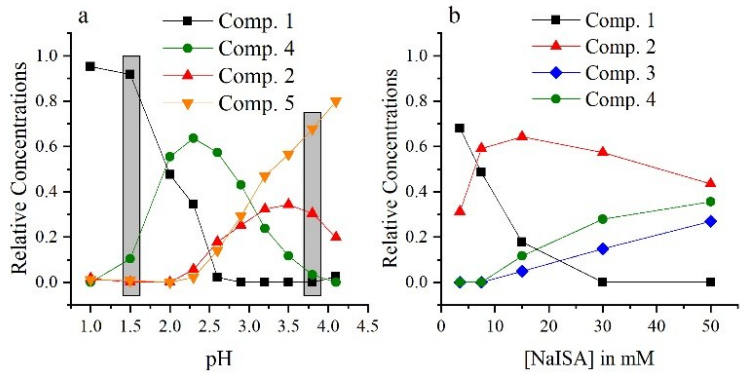

Fig. SI 41: Relative concentrations of the five components within the EXAFS pH- (a) and concentration-series (grey framed samples were not measured by EXAFS, but UV-Vis) (b). The concentration was determined by evaluating the corresponding UV-Vis spectra of the EXAFS samples with ITFA, using the single component spectra in Fig. SI 32 as references for the five components.

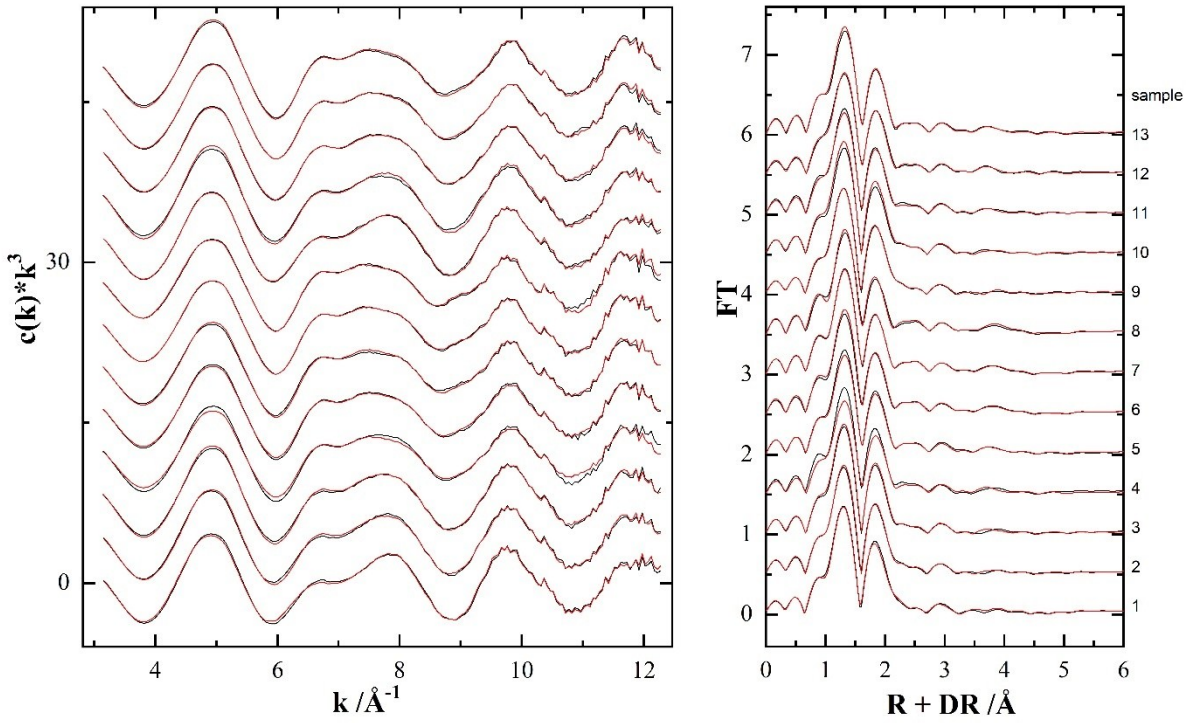

Fig. SI 42: U L_{III}-edge EXAFS spectra (left) and corresponding Fourier-transforms (FT) (right). Experimental data (black) and reconstructed data (red) by using the ITFA isolated spectra of the three components (Fig. SI 43) and their relative concentrations (Fig. 8 a). Sample numbers refer to Tab. SI 9.

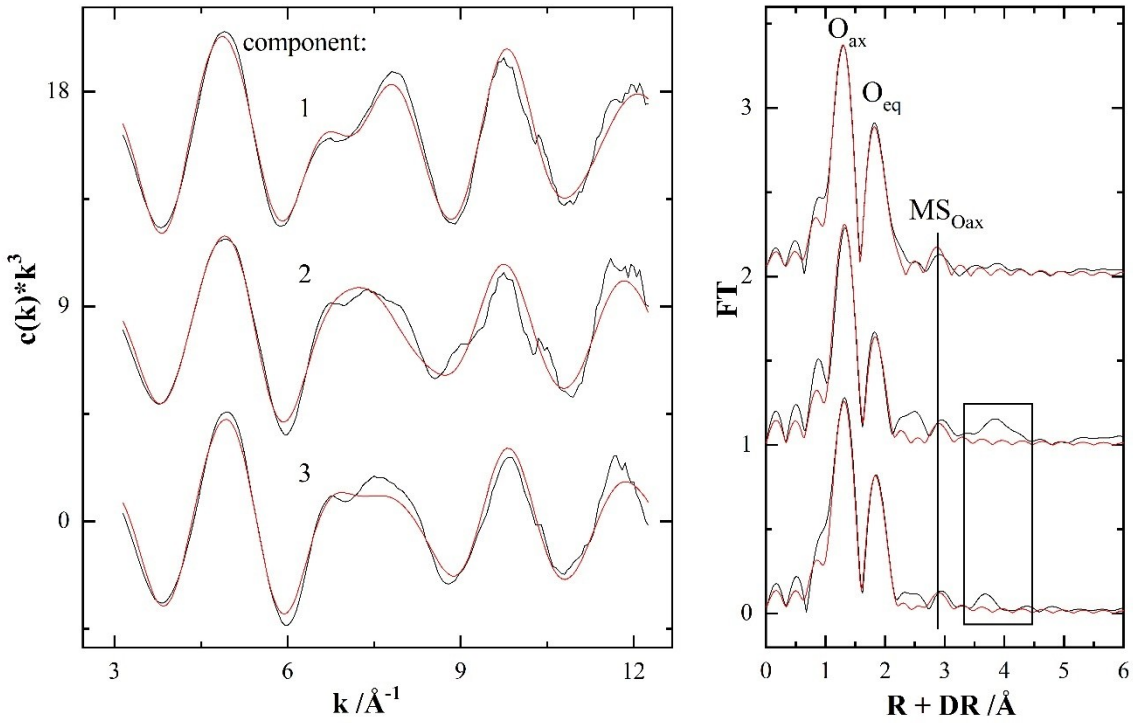

Fig. SI 43: U L_{III}-edge EXAFS spectra (left) and corresponding Fourier-transforms (FT) (right). ITFA isolated spectra (black) and shell fit (red). Assignments of FT features explained in the main text.

8 ITFA

If several metal species coexist in solution, then the measured signal represents a linear combination of the spectra of the single metal species weighted by their respective fractions so that the Beer-Lambert law can be employed as a linear mixing model (LMM). ITFA is a well-established tool aimed at the decomposition of the spectral mixtures into their spectral components based on a LMM.[8,9,18–20,10–17]

In the case of EXAFS the spectral components can also originate from the signals of atoms or groups of atoms, which change their spectral fraction as a function of a physico-chemical parameters like the pH or concentration.[10–12,20] In the first step of ITFA the c spectral mixtures are decomposed into a set of c eigenvectors, which enables a complete reconstruction of the spectral mixtures by their linear combination. However, only n eigenvectors contain useful spectral information, while c-n eigenvectors cover solely the experimental error like noise. The determination of n is accomplished by the semi-empirical indicator function (IND) which reaches a minimum at n.[21] In the second step the eigenvectors are transformed into a physically interpretable form by the VARIMAX procedure.[22] The resulting factor loadings allows a qualitative measure of the fractions of the spectral components. In the third step the spectra and the fractions of the components are isolated from the spectral mixtures by using the iterative target test (ITT).[23] For the ITT and in order to receive a unique solution n^2-n, fractions of the components must be given and fixed during the iteration.

9 Density difference plots

9.1 $[UO_2(ISA)(H_2O)_3]^+$ - 5-membered ring

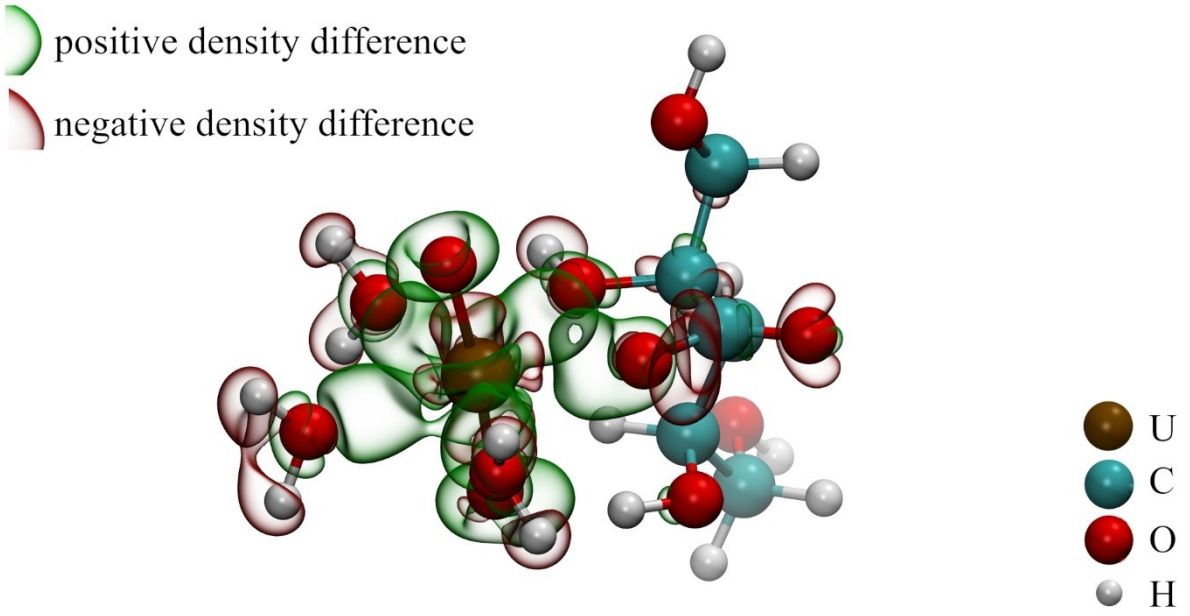

Fig. SI 44: Calculated electron density changes in a $[UO_2(ISA)(H_2O)_3]^+$ with 5-membered ring as binding motif (isovalues for the representation of electron densities were -0.005 (red) and +0.005 (green) (perspective one).

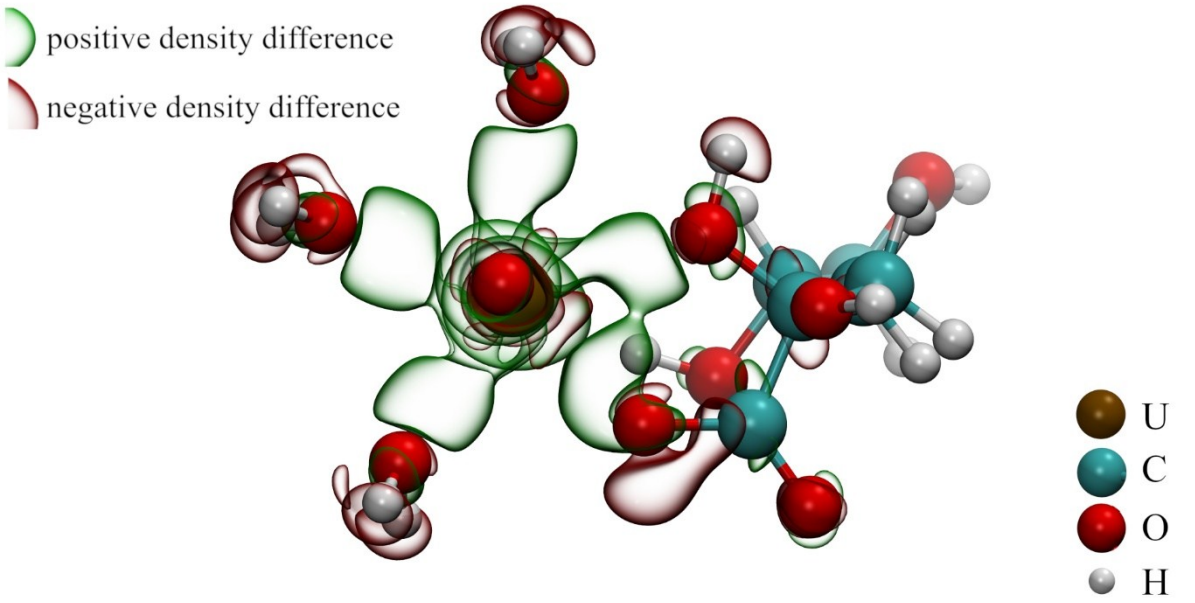

Fig. SI 45: Calculated electron density changes in a $[UO_2(ISA)(H_2O)_3]^+$ with 5-membered ring as binding motif (isovalues for the representation of electron densities were -0.005 (red) and +0.005 (green) (perspective two).

9.2 $[UO_2(ISA)(H_2O)_3]^+$ - 6-membered ring

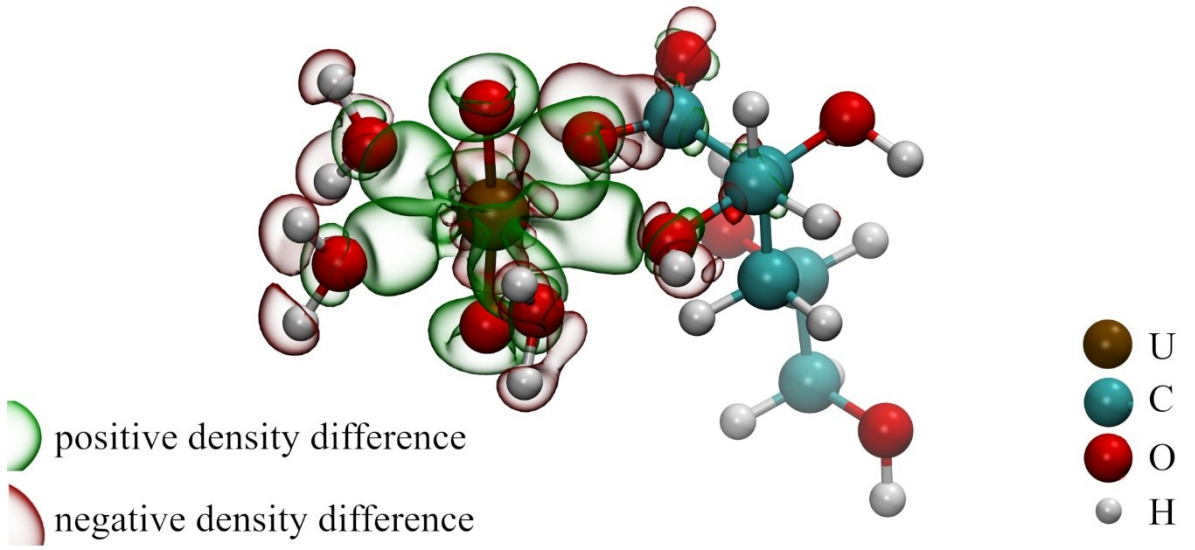

Fig. SI 46: Calculated electron density changes in a $[UO_2(ISA)(H_2O)_3]^+$ with 6-membered ring as binding motif (isovalues for the representation of electron densities were -0.005 (red) and +0.005 (green) (perspective one).

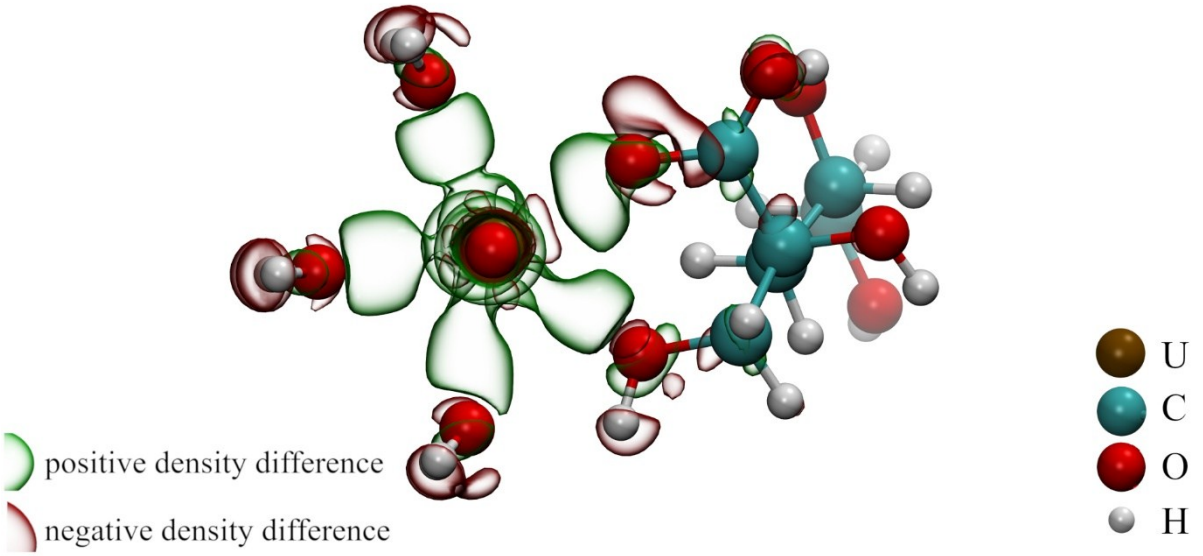

Fig. SI 47: Calculated electron density changes in a $[UO_2(ISA)(H_2O)_3]^+$ with 6-membered ring as binding motif (isovalues for the representation of electron densities were -0.005 (red) and +0.005 (green) (perspective two).

9.3 $[UO_2(ISA)_2(H_2O)]$ - 6-membered and 5-membered rings

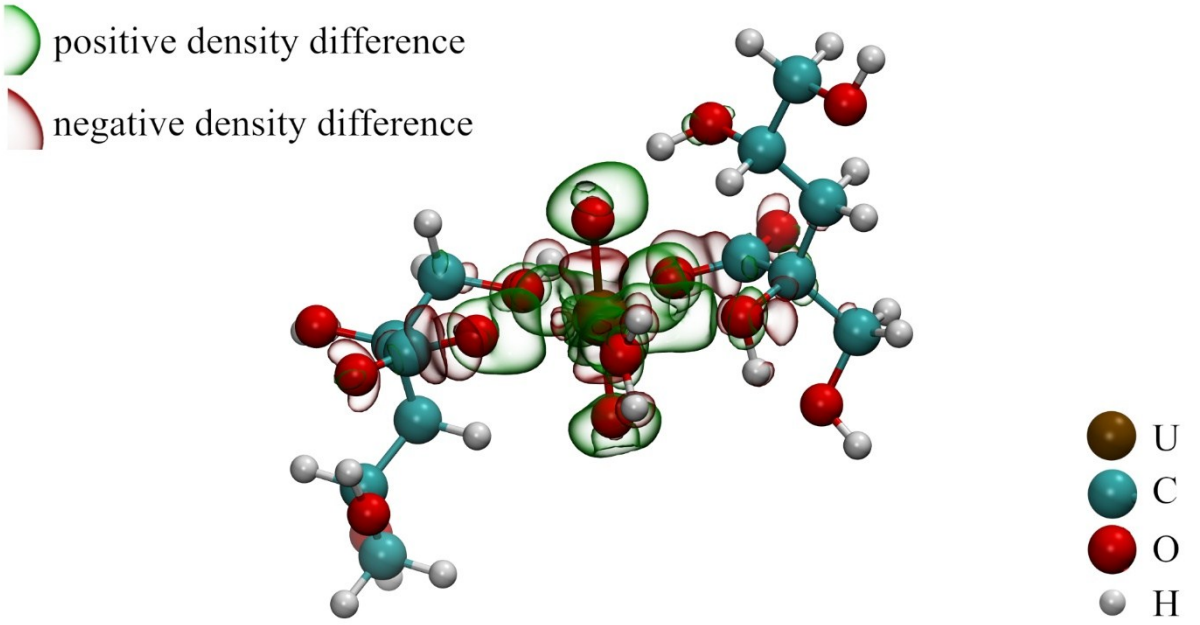

Fig. SI 48: Calculated electron density changes in a $[UO_2(ISA)_2(H_2O)]$ with 5- and 6-membered rings as binding motifs (isovalues for the representation of electron densities were -0.005 (red) and +0.005 (green) (perspective one).

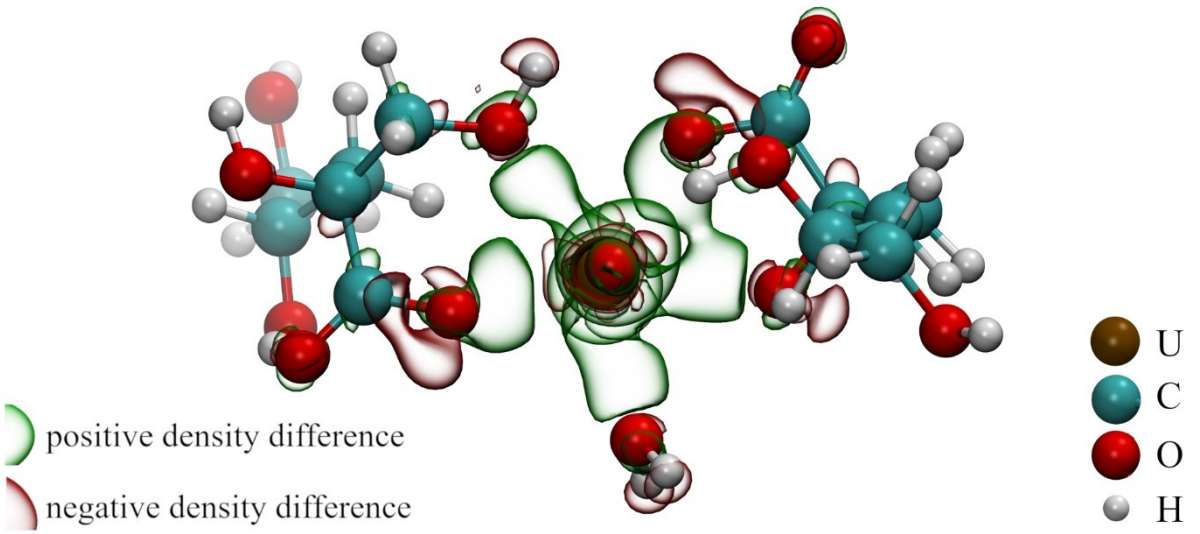

Fig. SI 49: Calculated electron density changes in a $[UO_2(ISA)_2(H_2O)]$ with 5- and 6-membered rings as binding motifs (isovalues for the representation of electron densities were -0.005 (red) and +0.005 (green) (perspective two).

9.4 $[(UO_2)_2(ISA)(H_2O)_6]^{3+}$ - 6-membered and 5-membered rings

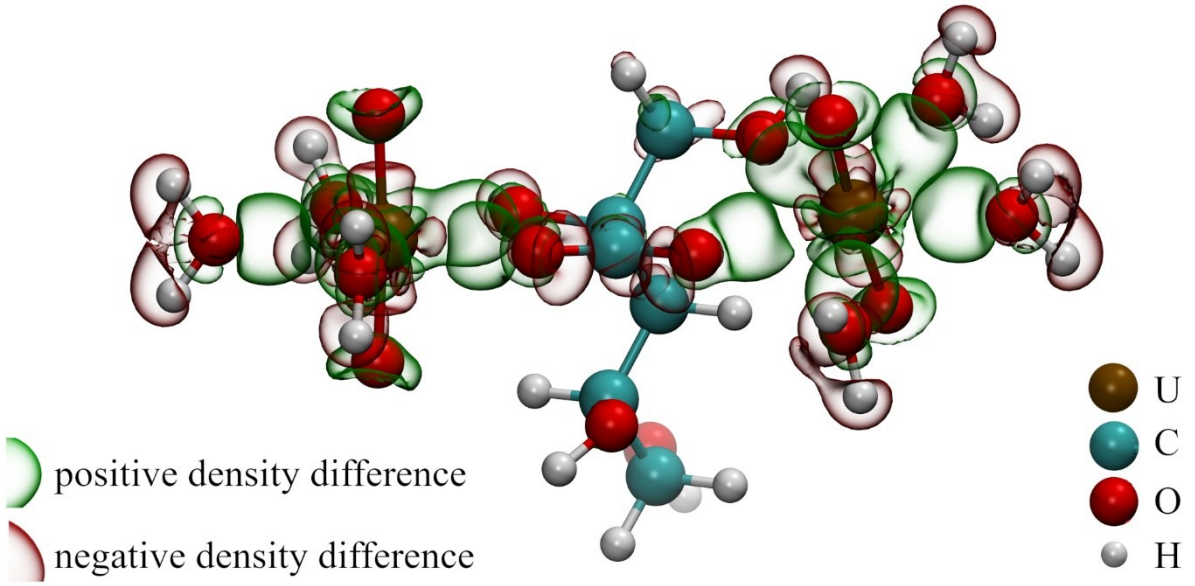

Fig. SI 50: Calculated electron density changes in a $[(UO_2)_2(ISA)(H_2O)_6]^{3+}$ with 5- and 6-membered rings as binding motifs (isovalues for the representation of electron densities were -0.005 (red) and +0.005 (green) (perspective one).

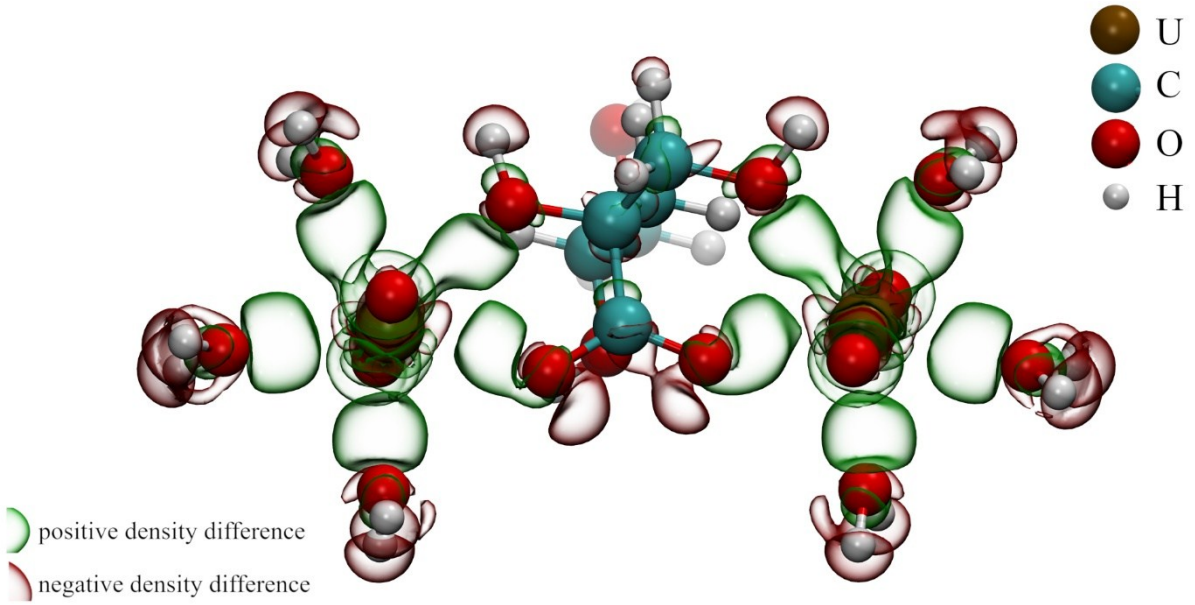

Fig. SI 51: Calculated electron density changes in a $[(UO_2)_2(ISA)(H_2O)_6]^{3+}$ with 5- and 6-membered rings as binding motifs (isovalues for the representation of electron densities were -0.005 (red) and +0.005 (green) (perspective two).

9.5 $[UO_2(HISA)(ISA)(H_2O)]^+$

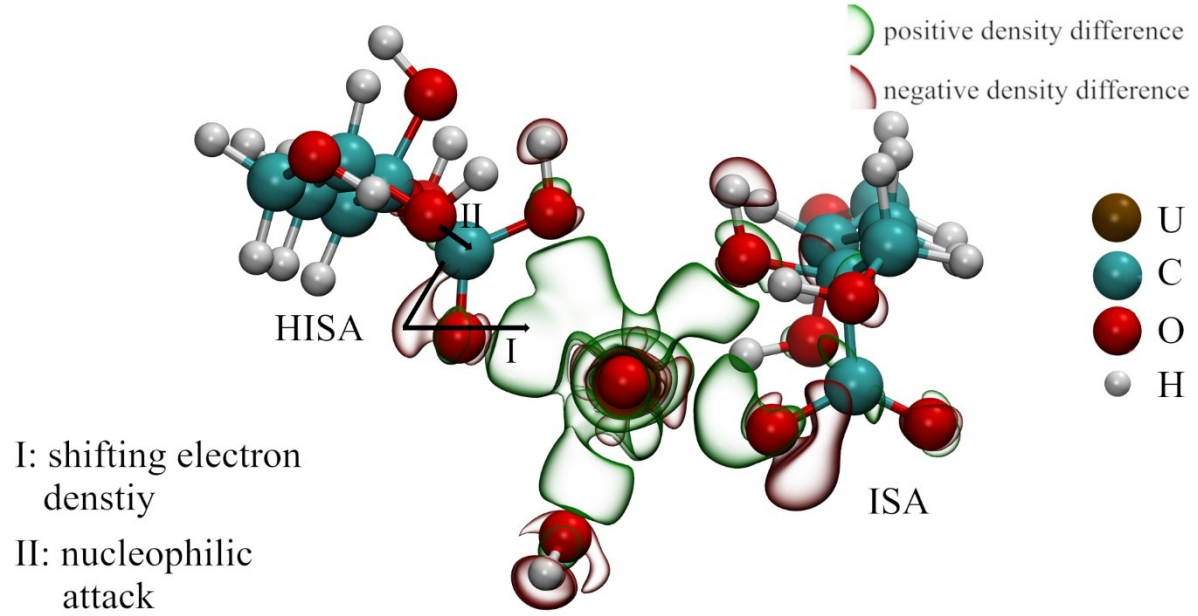

Fig. SI 52: Calculated electron density changes in a $[UO_2(HISA)(ISA)(H_2O)]^+$ complex and the impact on the lactone formation reaction (isovalues for the representation of electron densities were -0.005 (red) and +0.005 (green) (perspective two).

1 P. B. Shaw, 2013, 271.

2 H. Cho, D. Rai, N. J. Hess, Y. Xia and L. Rao, *J. Solution Chem.*, 2003, **32**, 691–702.

3 M. . Glaus, L. . van Loon, S. Achatz, A. Chodura and K. Fischer, *Anal. Chim. Acta*, 1999, **398**, 111–122.

4 R. Brückner, *Reaktionsmechanismen*, Springer Berlin Heidelberg, Berlin, Heidelberg, 2004, vol. 91.

5 J. M. Chalmers and P. R. Griffiths, *Handbook of Vibrational Spectroscopy*, 2002.

6 G. Cassanas, M. Morssli, E. Fabrègue and L. Bardet, *J. Raman Spectrosc.*, 1991, **22**, 409–413.

7 J.-J. Max and C. Chapados, *J. Phys. Chem. A*, 2004, **108**, 3324–3337.

8 C. Lucks, A. Rossberg, S. Tsushima, H. Foerstendorf, A. C. Scheinost and G. Bernhard, *Inorg. Chem.*, 2012, **51**, 12288–12300.

9 E. Breynaert, A. C. Scheinost, D. Dom, A. Rossberg, J. Vancluysen, E. Gobechiya, C. E. A. Kirschhock and A. Maes, *Environ. Sci. Technol.*, 2010, **44**, 6649–6655.

10 D. R. Fröhlich, A. Kremleva, A. Rossberg, A. Skerencak-Frech, C. Koke, S. Krüger, N. Rösch and P. J. Panak, *Inorg. Chem.*, 2017, **56**, 6820–6829.

11 D. R. Fröhlich, A. Skerencak-Frech, N. Bauer, A. Rossberg and P. J. Panak, *J. Synchrotron Radiat.*, 2015, **22**, 99–104.

12 D. R. Fröhlich, A. Skerencak-Frech, U. Kaplan, C. Koke, A. Rossberg and P. J. Panak, *J. Synchrotron Radiat.*, 2015, **22**, 1469–1474.

13 A. Ikeda, C. Hennig, A. Rossberg, S. Tsushima, A. C. Scheinost and G. Bernhard, *Anal. Chem.*, 2008, **80**, 1102–1110.

14 R. Kirsch, D. Fellhauer, M. Altmaier, V. Neck, A. Rossberg, T. Fanghänel, L. Charlet and A. C. Scheinost, *Environ. Sci. Technol.*, 2011, **45**, 7267–7274.

15 I. Pidchenko, K. O. Kvashnina, T. Yokosawa, N. Finck, S. Bahl, D. Schild, R. Polly, E. Bohnert, A. Rossberg, J. Göttlicher, K. Dardenne, J. Rothe, T. Schäfer, H. Geckeis and T. Vitova, *Environ. Sci. Technol.*, 2017, **51**, 2217–2225.

16 A. Rossberg, T. Abe, K. Okuwaki, A. Barkleit, K. Fukuzawa, T. Nakano, Y. Mochizuki and S. Tsushima, *Chem. Commun.*, 2019, **55**, 2015–2018.

17 A. Rossberg, K.-U. Ulrich, S. Weiss, S. Tsushima, T. Hiemstra and A. C. Scheinost, *Environ. Sci. Technol.*, 2009, **43**, 1400–1406.

18 A. C. Scheinost, A. Rossberg, D. Vantelon, I. Xifra, R. Kretzschmar, A.-K. Leuz, H. Funke and C. A. Johnson, *Geochim. Cosmochim. Acta*, 2006, **70**, 3299–3312.

19 K.-U. Ulrich, A. Rossberg, H. Foerstendorf, H. Zänker and A. C. Scheinost, *Geochim. Cosmochim. Acta*, 2006, **70**, 5469–5487.

20 F. Taube, B. Drobot, A. Rossberg, H. Foerstendorf, M. Acker, M. Patzschke, M. Trumm, S. Taut and T. Stumpf, *Inorg. Chem.*, 2019, **58**, 368–381.

21 E. R. Malinowski, *Anal. Chem.*, 1977, **49**, 612–617.

22 H. F. Kaiser, *Psychometrika*, 1958, **23**, 187–200.

23 T. H. Brayden, P. A. Poropatic and J. L. Watanabe, *Anal. Chem.*, 1988, **60**, 1154–1158.